RSC Advances

REVIEW

View Article Online
View Journal | View Issue

Cite this: *RSC Adv.*, 2025, **15**, 37609

Push–pull heterocycles and beyond: recent developments in absorption, emission, and ICT properties

Manel Essid[a] and Ehsan Ullah Mughal *[b]

Heterocyclic scaffolds represent a cornerstone in the development of advanced organic materials owing to their tunable electronic structures and diverse photophysical properties. Recent studies have demonstrated significant progress in the design and synthesis of heterocyclic chromophores, particularly focusing on their absorption and emission behaviors, donor–acceptor interactions, intramolecular charge transfer (ICT), and solvent-dependent spectral shifts. In this review, we present for the first time a comprehensive summary of the literature reported during 2024–2025, covering a wide range of systems including indole–coumarins, 3-cyano-2-pyridones, tetracyanobuta-1,3-diene (TCBD) derivatives, highly annulated boron-dipyrromethenes (BODIPYs) and pyrimidine-based boron complexes. Key discussions emphasize how structural modifications, solvent polarity, and push–pull effects influence band gaps, bathochromic and hypsochromic shifts, fluorescence quantum yields, and near-infrared (NIR) emission properties. By correlating structure–property relationships, this review provides important insights into molecular design strategies and highlights the potential of heterocyclic chromophores as promising candidates for next-generation optoelectronic, sensing, and photonic applications.

Received 3rd September 2025
Accepted 2nd October 2025

DOI: 10.1039/d5ra06623a

rsc.li/rsc-advances

[a]*Chemistry Department, College of Science, King Khalid University (KKU), P.O. Box 9004, Abha 61413, Saudi Arabia*

[b]*Department of Chemistry, University of Gujrat, Gujrat-50700, Pakistan. E-mail: ehsan.ullah@uog.edu.pk*

Ehsan Ullah Mughal

Ehsan Ullah Mughal received his PhD in Organic Chemistry from Bielefeld University, Germany, in 2013. Currently, he is working as Tenured Associate Professor in Department of Chemistry, University of Gujrat, Pakistan. He was a post doc fellow at Max-Planck Institute for Polymer Research, Mainz, Germany from 2013 to 2014. His current research interests include the design and synthesis of bioactive heterocycles, synthetic flavonoids, transition metal-based terpyridine complexes and their uses in the fabrication of DSSCs and as efficient photocatalysts. His research in the field has resulted in more than 120 published articles (research papers and review papers) in reputable high impact journals. His publications have made a great impact in the field by receiving more than 2910 citations with h-index of 31.

1 Introduction

The development of functional organic molecules with tailored optical and electronic properties has gained significant attention over the past decades due to their extensive application in optoelectronics, photovoltaics, sensing, and bioimaging technologies. Among these, push–pull systems, also referred to as donor–acceptor (D–A) architectures, represent a versatile class of molecular frameworks that exhibit remarkable photophysical behavior arising from ICT phenomena.[1–3]

Push–pull molecules are typically characterized by the presence of an electron-rich donor moiety (D) and an electron-deficient acceptor moiety (A), interconnected through a π-conjugated system. This configuration facilitates delocalization of π-electrons and promotes directional charge separation upon excitation.[4,5] The resulting ICT leads to properties such as strong solvatochromism, tunable absorption/emission wavelengths, enhanced nonlinear optical (NLO) responses, and efficient charge transport—making them attractive candidates for next-generation optoelectronic materials.[6,7]

Heterocyclic cores, especially those containing nitrogen, oxygen, or sulfur atoms, offer a privileged structural motif for designing push–pull systems. These heterocycles not only contribute to conjugation but also provide electronic tunability through substituent modification and heteroatom variation.[8,9] Examples include thiophene, pyrrole, indole, benzothiadiazole, and triazole scaffolds, which have been widely employed in

organic light-emitting diodes (OLEDs), dye-sensitized solar cells (DSSCs), and fluorescent chemosensors.[10–13]

In this review, we aim to present a comprehensive analysis of the photophysical characterization, and applications of push–pull heterocyclic scaffolds. The interplay between molecular structure and optical behavior will be emphasized, along with recent developments and emerging trends in the field.

2 Fundamentals of push–pull systems

Push–pull molecular systems, often described as D–A frameworks, are designed to promote ICT through the strategic arrangement of electron-donating and electron-withdrawing units connected by a π-conjugated backbone.[14] These systems have attracted intense interest due to their unique photophysical and optoelectronic properties, which are highly tunable based on structural modifications.[15,16]

2.1 Electronic structure and charge transfer

In a typical D–A molecule, the donor group contributes electron density through resonance or inductive effects, whereas the acceptor withdraws electron density. Upon photoexcitation, an electron is promoted from the highest occupied molecular orbital (HOMO), which is localized predominantly on the donor, to the lowest unoccupied molecular orbital (LUMO), localized on the acceptor. This process leads to a polarized excited state with a significant dipole moment, promoting charge separation and red-shifted absorption/emission spectra.[2,17,18] Such ICT transitions are responsible for the bathochromic shift in UV-vis spectra and large Stokes shifts in fluorescence, especially in polar solvents. Moreover, the HOMO–LUMO gap can be effectively modulated by changing the strength of the donor and acceptor groups and the π-conjugated bridge length.[19–21]

The charge-transfer (CT) phenomenon can be broadly classified into two types: intermolecular and ICT. Intermolecular CT involves the transfer of charge from an electron-rich donor unit to an electron-deficient acceptor unit located on separate molecules. In contrast, ICT occurs when both donor and acceptor moieties are present within the same molecular framework. ICT typically takes place in the photoexcited state upon absorption of light at an appropriate wavelength. In this state, the electron density distribution differs significantly from that of the ground state, as excitation promotes electron migration from the donor to the acceptor region within the molecule. When the donor and acceptor groups are connected *via* a π-conjugated bridge, through-bond ICT occurs. Alternatively, through-space ICT may take place when conjugation is interrupted but the donor and acceptor groups are spatially aligned to facilitate charge transfer. Although through-space CT

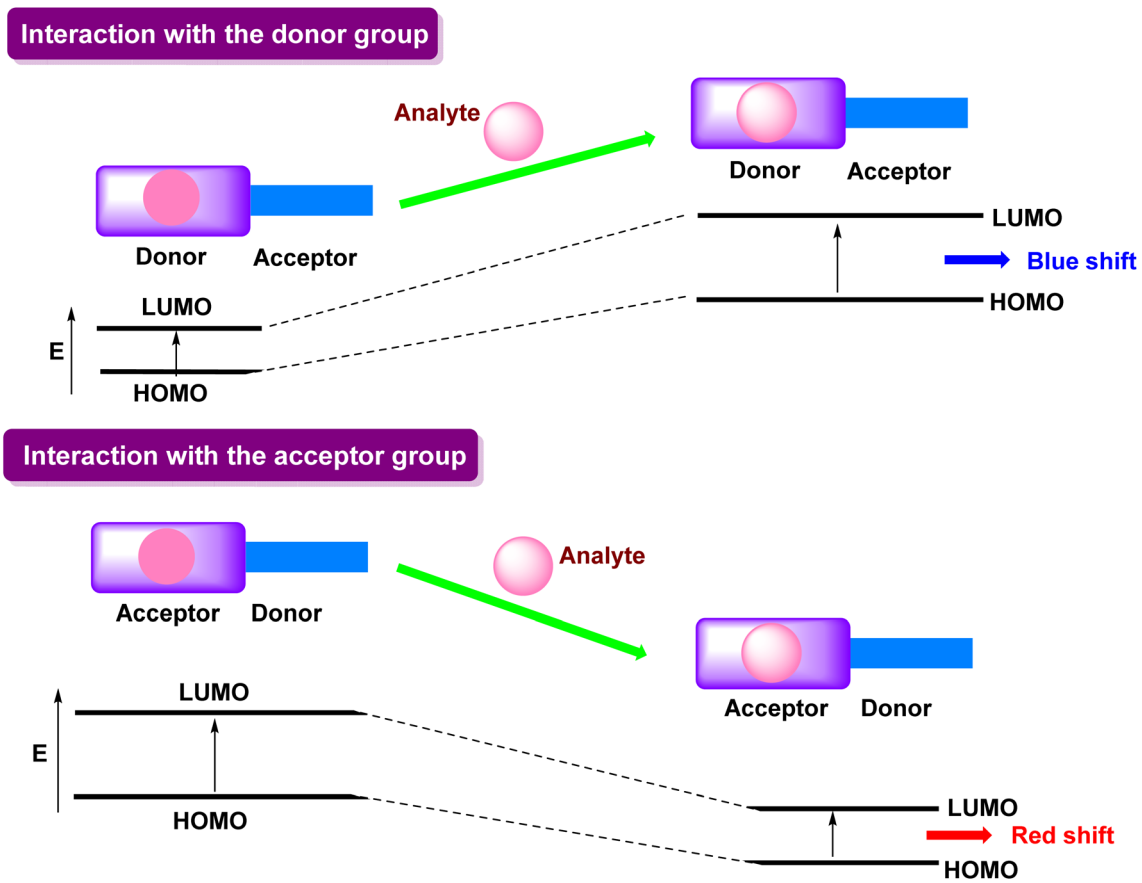

Fig. 1 Schematic representation of the ICT process employed in sensing systems. Reproduced from ref. 21 with permission from Royal Society of Chemistry, under the terms of the CC (BY-NC) 3.0 license, Copyright © 2018.

is common in π-stacked systems through intermolecular interactions, intramolecular through-space ICT has been less extensively studied.[22]

ICT processes are typically associated with distinct photophysical changes, including variations in dipole moment and pronounced Stokes shifts. Interaction of a cation with an electron-donating group reduces its donor strength and conjugation, leading to a blue shift in the emission spectrum and a decrease in molar extinction coefficient. In contrast, interaction with an electron-withdrawing group enhances acceptor strength, resulting in a red shift and increased molar extinction coefficient.[23]

The concept of employing ICT for cation sensing was first introduced by Valeur, where fluorescent probes were designed by linking electron-donating and electron-accepting groups within a single molecule to form a "push–pull" π-electron system in the excited state. Such systems exhibit sensitive optical responses: interaction of an analyte with the donor unit leads to a hypsochromic (blue) shift in the absorption spectrum, whereas interaction with the acceptor unit induces a bathochromic (red) shift. These spectral changes are often accompanied by variations in fluorescence lifetimes and quantum yields, making ICT-based probes valuable tools for selective and sensitive cation detection (Fig. 1).[21]

Upon photoexcitation, the molecule in its enol form (*E*) absorbs a photon and undergoes a transition from the ground state (S_0) to the excited state (S_1, *E**). In the excited state, a proton transfer occurs through intramolecular hydrogen bonding, generating the *keto tautomer in the excited state (K**). This process is known as Excited-State Intramolecular Proton Transfer (ESIPT). The excited keto tautomer (K*) can then undergo radiative decay, emitting fluorescence at a longer wavelength compared to the absorption band, typically resulting in a large Stokes shift. After emission, the molecule relaxes back to the ground-state keto form (K). Subsequently, a Ground-State Intramolecular Proton Transfer (GSIPT) occurs, in which the proton transfers back to regenerate the enol form (*E*) through hydrogen-bond reorganization.[24,25] This GSIPT step completes the ESIPT–GSIPT photocycle (Fig. 2).

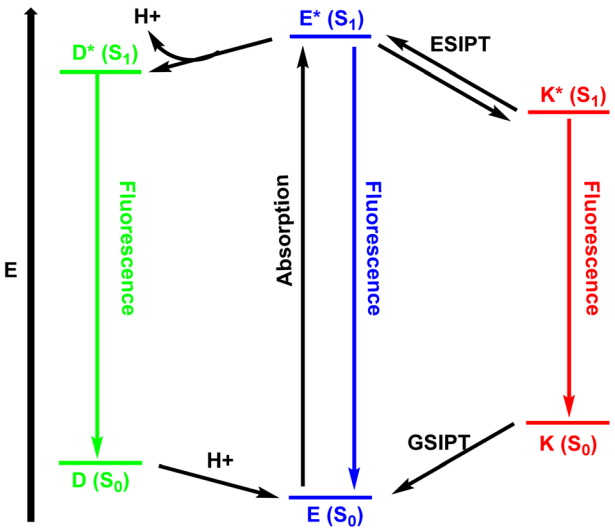

Fig. 2 Schematic representation of ESIPT process. Reproduced from ref. 25 with permission from Royal Society of Chemistry, under the terms of the CC (BY-NC) 3.0 license, Copyright © 2024.

2.2 Solvatochromism and dipole moment effects

Solvatochromism—changes in absorption or emission wavelengths with solvent polarity—is a hallmark of push–pull chromophores. These shifts are generally classified as positive solvatochromism (red shift with increasing solvent polarity) due to the stabilization of the excited ICT state in polar media.[26,27] The Lippert–Mataga equation is often applied to quantify the correlation between the dipole moment difference and solvent-dependent emission maxima. The increased dipole moment in the excited state leads to solvent–solute interactions, further lowering the energy of the excited state and increasing the wavelength of emission (Fig. 3). Molecules with large dipole moments in their excited states also exhibit significant second-order NLO responses.[28]

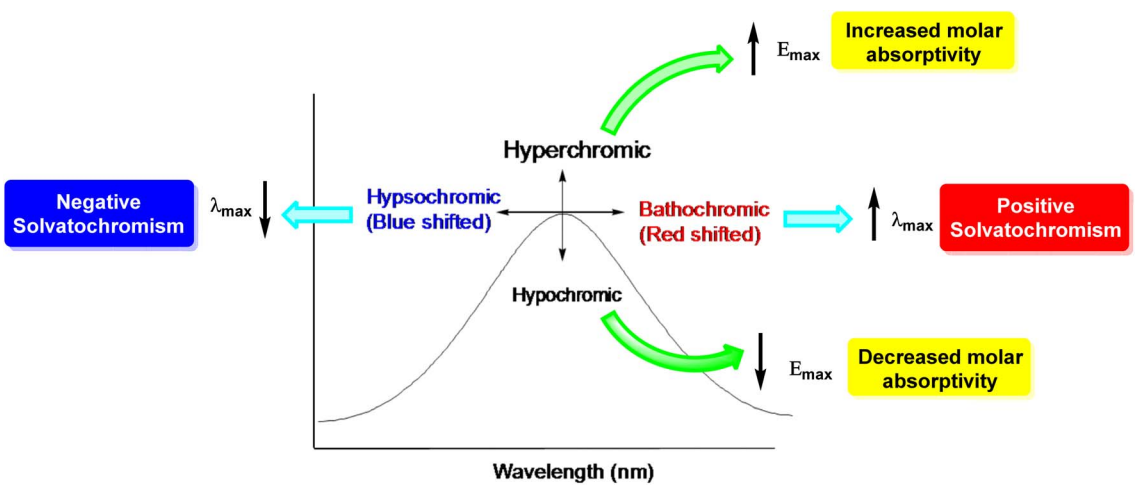

Fig. 3 Solvatochromic behavior of the push–pull heterocyclic chromophore.

2.3 Role of conjugation and molecular planarity

The extent of π-conjugation directly influences the delocalization of charge carriers. A planar geometry allows efficient overlap of p-orbitals along the conjugated chain, which facilitates charge delocalization and reduces the energy gap. On the other hand, steric hindrance or torsional strain may disrupt planarity and thus impair charge transfer efficiency.[29] Planar and rigid systems also enhance photostability and quantum yields, making them more suitable for solid-state applications such as OLEDs and field-effect transistors (OFETs).[30] However, twisted intramolecular charge transfer (TICT) states can also emerge in molecules with flexible π-systems, often resulting in dual emission behavior or aggregation-induced emission (AIE) phenomena.[31,32]

2.4 Design implications

Understanding the fundamental electronic interactions between the donor, bridge, and acceptor units allows rational design of molecules with desired properties (Fig. 4).[33] For instance, replacing a weak donor with a strong one (*e.g.*, replacing methoxy with dimethylamino) results in an upward shift in HOMO energy, while introducing electron-deficient moieties (*e.g.*, cyano, nitro, triazine) lowers the LUMO, effectively narrowing the band gap.[34] This tunability is critical for customizing materials for specific roles such as NIR emitters, photovoltaic dyes, or bioimaging agents.

3 Common heterocyclic scaffolds in push–pull systems

Heterocycles play a pivotal role in modern organic materials chemistry due to their inherent aromaticity, electronic versatility, and ease of functionalization.[35,36] In push–pull systems, heterocyclic scaffolds serve either as electron donors, acceptors, or bridging π-spacers. Their heteroatoms—nitrogen, sulfur, or oxygen—significantly influence the molecular orbitals and the efficiency of ICT (Fig. 5).[37] This section categorizes key heterocycles based on their donor–acceptor roles and discusses representative scaffolds commonly employed in donor–π–acceptor (D–π–A) molecular architectures[38] (Table 1).

3.1 Electron-donating heterocycles

3.1.1 Thiophene and oligothiophenes. Thiophene is one of the most widely studied π-conjugated heterocycles due to its planarity, electron-rich nature, and strong π–π stacking. In D–π–A systems, thiophene and its oligomers (*e.g.*, bithiophene, terthiophene) act as excellent donor moieties and π-bridges that enhance conjugation and electronic delocalization. Their high HOMO levels and oxidative stability make them ideal for light-absorbing and charge-transporting systems.[39–42]

3.1.2 Pyrrole and carbazole. Pyrrole-containing systems exhibit high electron density due to the lone pair on nitrogen, making them effective donors in push–pull systems. Carbazole, a rigid and planar tricyclic derivative of pyrrole, is another common electron donor in optoelectronic materials. It provides strong thermal and photochemical stability along with hole-transporting ability.[43–45]

3.1.3 Indole and its derivatives. Indole and its fused analogs, including benzofuran and benzo[*b*]thiophene, possess extended conjugation and moderate donor properties. Substitution at the nitrogen atom can fine-tune their electron-donating capacity, allowing structural diversity in D–π–A materials.[46–48]

3.2 Electron-accepting heterocycles

3.2.1 Benzothiadiazole (BTD). Benzothiadiazole is a well-established electron acceptor due to its high electronegativity and strong electron-withdrawing character imparted by the diazole ring. Its incorporation in the acceptor unit leads to

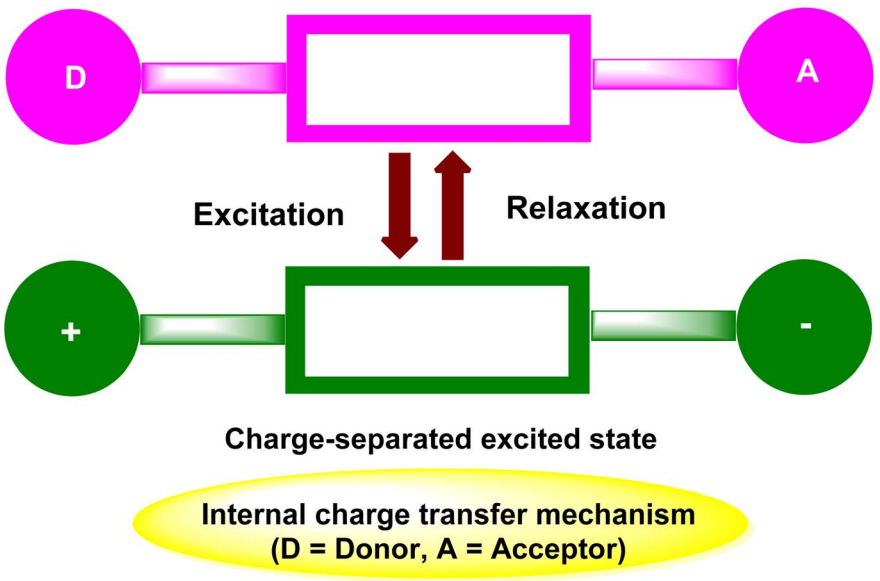

Fig. 4 Schematic illustration of the ICT mechanism in a push–pull heterocyclic chromophore.

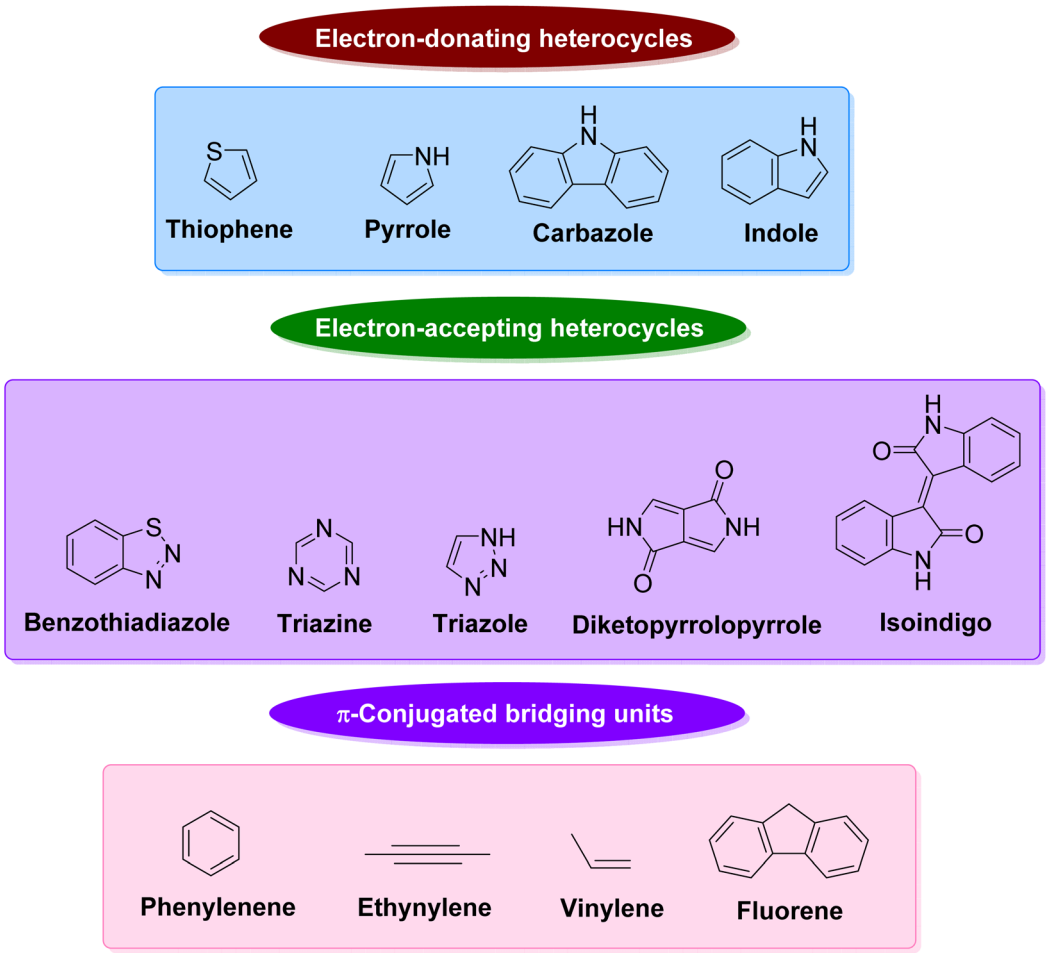

Fig. 5 Chemical structure of various heterocycles.

Table 1 Examples of heterocyclic compounds

Heterocycle	Role in D–π–A system	Application
Thiophene	Donor/π-bridge	DSSCs, OLEDs
Carbazole	Donor	TADF emitters, FETs
Benzothiadiazole	Acceptor	DSSCs, NLO materials
Triazole	Acceptor/bridge	Fluorescent sensors, click-dyes
DPP	Strong acceptor	Organic solar cells, transistors

enhanced ICT and lower LUMO energy levels, making BTD-based dyes suitable for DSSCs, OLEDs, and FETs.[49]

3.2.2 Triazines and triazoles. Triazine derivatives (*s*-triazine and heptazine) are potent acceptors because of the presence of three nitrogen atoms. Similarly, 1,2,3-triazoles formed *via* click chemistry provide electron-deficient cores and synthetic versatility. Their inclusion in D–π–A systems enhances electron affinity and photochemical robustness.[50,51]

3.2.3 Isoindigo and diketopyrrolopyrrole (DPP). These extended π-systems incorporate carbonyl and electron-withdrawing nitrogen atoms that facilitate efficient charge transport. DPP, in particular, has emerged as a "universal acceptor" in push–pull polymers due to its excellent planarity, stability, and strong ICT transitions.[52]

3.3 π-Conjugated bridging units

In many cases, heterocycles act as π-bridging spacers to mediate charge transfer between the donor and acceptor units. Common examples include phenylene, ethynylene, vinylene, fluorene, and fused systems such as thiadiazoloquinoxaline. These bridges influence the rigidity, planarity, and dihedral angle of the entire molecular scaffold, which in turn modulates the photophysical response.[34,53]

4 Photophysical properties of push–pull heterocyclic scaffolds

Push–pull heterocyclic systems exhibit rich photophysical behavior owing to their polarized π-conjugated architectures.

These systems undergo significant ICT, which profoundly influences their optical absorption, emission, solvatochromism, and excited-state dynamics. This section explores their key photophysical properties in the context of electronic structure, substituent effects, and solvent polarity.

4.1 Absorption and emission characteristics

Push–pull heterocycles typically display strong absorption in the UV-vis region, primarily arising from π–π* and ICT transitions. The donor–π–acceptor (D–π–A) arrangement facilitates a bathochromic shift (red shift) in absorption and emission bands due to increased electron delocalization. Strong donors (*e.g.*, *N*,*N*-dialkylamines) and potent acceptors (*e.g.*, –CN, –NO_2, –CHO) intensify the ICT band and reduce the HOMO–LUMO energy gap. Fluorescence quantum yields vary significantly depending on the nature of the donor and acceptor and their rigidity.[54,55]

4.2 Solvatochromism and polarity dependence

Push–pull heterocycles often display positive solvatochromism—a red shift in emission with increasing solvent polarity—due to stabilization of the excited-state dipole. This phenomenon is quantified using Lippert–Mataga plots, which relate the Stokes shift to solvent polarity function. Compounds with strong ICT show large solvatochromic shifts, making them suitable for polarity probes and environment-sensitive fluorophores.[56]

4.3 Two-photon absorption (TPA)

Two-photon absorption (TPA) is a nonlinear optical (NLO) process in which two photons are absorbed simultaneously to promote a molecule from the ground to an excited electronic state. Push–pull heterocyclic systems, characterized by electron donor (D) and acceptor (A) groups connected through π-conjugated bridges, are particularly promising for TPA applications due to their strong ICT and high molecular polarizability. However, TPA cross-sections (δ) are not determined solely by the donor–acceptor strength; they arise from a complex interplay of structural, electronic, and environmental factors that govern electronic coupling and excited-state dynamics.

The electronic coupling between donor and acceptor units through conjugated bridges plays a decisive role in determining both the magnitude of δ and the nature of the excited states involved. Extended π-conjugation and rigid, planar geometries generally enhance the delocalization of frontier orbitals, leading to increased transition dipole moments and larger δ values. Additionally, molecular symmetry affects charge redistribution upon excitation: quadrupolar architectures (D–π–A–π–D) often display stronger TPA responses than dipolar systems. The energy gap between ground and excited states, and resonance with virtual intermediate states, further modulate the two-photon transition probability. Moreover, solvent polarity and environmental effects stabilize ICT states, influencing the balance between local excitation (LE) and ICT contributions, which can either enhance or suppress TPA.[57]

Below, we summarize the key factors that govern TPA properties in push–pull heterocyclic systems, along with representative examples.

4.3.1 Donor–acceptor strength and ICT extent. Strong donor and acceptor groups enhance ICT and often increase δ values. Thiophene-based D–π–A–π–D systems containing *N*,*N*-dialkylaniline donors and dicyanovinyl acceptors exhibited δ values exceeding 1500 GM at 800 nm, attributed to their strong push–pull character and planar conjugation.[58] Similarly, benzothiadiazole-based π-bridges combined with julolidine donors afforded δ values in the 1000–2000 GM range, illustrating the impact of strong D–A pairs.[59]

4.3.2 π-Conjugation length and molecular planarity. Extended π-bridges promote frontier orbital delocalization, resulting in larger transition dipole moments and enhanced two-photon transition probabilities. Oligothiophene-based chromophores showed a systematic increase in δ from 350 GM ($n = 1$) to 1800 GM ($n = 4$) with increasing bridge length.[60] Likewise, planar benzofuran–benzothiadiazole systems exhibited higher δ values than their twisted analogues due to more efficient orbital overlap.[61]

4.3.3 Molecular symmetry and topology. Quadrupolar (D–π–A–π–D) and octupolar (branched) structures typically show larger TPA cr1oss-sections than simple dipolar D–π–A systems because of cooperative charge transfer. Branched triphenylamine–benzothiadiazole systems with octupolar symmetry displayed δ values > 3000 GM at 800 nm, nearly double those of their dipolar counterparts.[62] Similarly, bis-donor D–π–A–π–D chromophores exhibit broadened TPA spectra and higher δ due to enha1nced charge resonance.[63]

4.3.4 Electronic coupling and substitution patterns. The nature of linkers and substitution patterns affects the electronic communication between D and A fragments. Fluorene-linked push–pull chromophores showed stronger TPA compared to phenylene-linked analogues, attributed to improved orbital overlap and conjugation efficiency.[64] *Meta*-linked donor–acceptor systems generally exhibit lower δ values than *para*-linked ones due to reduced π-delocalization.[63]

4.3.5 Solvent and environmental effects. Solvent polarity and aggregation can substantially influence TPA behavior. Polar solvents stabilize ICT states, often leading to red-shifted TPA maxima and increased δ values.[65] In some systems, aggregation-induced planarization enhances conjugation and δ. For example, cyanine-based chromophores exhibited over a twofold increase in δ upon aggregation, attributed to restricted intramolecular rotation and enhanced ICT.[66]

Push–pull heterocyclic chromophores with large TPA cross-sections are being exploited in multiphoton bioimaging, two-photon excited fluorescence microscopy, photodynamic therapy, and 3D optical data storage. Benzothiadiazole–triphenylamine chromophores with δ > 2500 GM have been successfully used for live cell imaging,[67] while cyano-substituted fluorene derivatives have been applied in high-resolution 3D data storage.[68]

4.4 Fluorescence lifetimes and excited-state behavior

Time-resolved photoluminescence measurements reveal details about excited-state deactivation pathways: short lifetimes (~ns) are characteristic of prompt fluorescence. Longer-lived states can suggest the presence of thermally activated delayed fluorescence (TADF) or intersystem crossing (ISC) to triplet states. Introduction of heteroatoms (N, O, S) facilitates ISC and can promote phosphorescence or TADF, especially in donor–acceptor rigid systems.[69]

4.5 Aggregation-induced emission (AIE) and solid-state effects

While many push–pull chromophores undergo aggregation-caused quenching (ACQ), some are designed with rotor-like or twisted geometries to enable AIE.[33,70] Such behavior is useful in solid-state emitters, chemosensors, and OLEDs.[71] Restriction of intramolecular motion in the aggregated state promotes radiative decay.[72–74]

4.6 Electrochemical and optical band gaps

Electrochemical studies (*e.g.*, cyclic voltammetry) complement photophysical analysis by revealing HOMO–LUMO levels: optical band gaps (from UV-vis onset) and redox potentials provide insight into charge transport properties. These data are essential for tuning materials for organic electronics, OPVs, and OLEDs.[75,76]

5. Applications of push–pull heterocycles in advanced materials

Push–pull heterocyclic scaffolds, with their tunable electronic properties and diverse photophysical behavior, have found a broad range of applications in advanced material science.[77] Their ability to undergo ICT and exhibit NLO responses makes them suitable for devices that rely on light absorption, emission, and charge transport. Below are key areas where these molecules have demonstrated significant potential[78] (Fig. 6).

5.1 Organic light-emitting diodes (OLEDs)

Push–pull compounds have emerged as efficient emissive layers in OLEDs, especially in the development of materials exhibiting TADF.[79] The spatial separation of HOMO and LUMO facilitates small singlet–triplet energy gaps (ΔE_{ST}), promoting efficient reverse intersystem crossing (RISC). Heterocyclic donors (*e.g.*, carbazole, phenoxazine) and acceptors (*e.g.*, benzothiadiazole, triazine) have been widely incorporated into TADF emitters. Example: triazine-based push–pull emitters achieved high external quantum efficiencies (EQEs) exceeding 25% in blue OLEDs.[80]

5.2 Organic photovoltaics (OPVs)

In OPVs, push–pull systems act as donor materials or non-fullerene acceptors: the D–π–A motif enhances light-harvesting over a broad spectral range and facilitates exciton dissociation. Electron-rich cores (*e.g.*, thiophene, dithienosilole) and acceptor end groups (*e.g.*, cyanoacrylic acid) are common. Push–pull small molecules or polymers enable fine-tuning of HOMO/LUMO levels for optimal energy level alignment with acceptors.[81]

5.3 Nonlinear optical (NLO) materials

Push–pull molecules with extended conjugation show pronounced second- and third-order nonlinearities, making them attractive for NLO applications: typical uses include optical switches, data storage, and frequency doubling (SHG). NLO efficiency is boosted in systems with rigid planarity and strong donor–acceptor contrast.[82]

5.4 Fluorescent probes and bioimaging

The environmental sensitivity of push–pull fluorophores makes them ideal for bioimaging and sensing: ICT-based fluorophores respond to solvent polarity, pH, metal ions, and biomolecular interactions. Such systems offer high contrast imaging with tunable emission wavelengths from blue to NIR. Example: D–A–D fluorophores with thiophene bridges have been used for lysosomal targeting and real-time intracellular pH monitoring.[83]

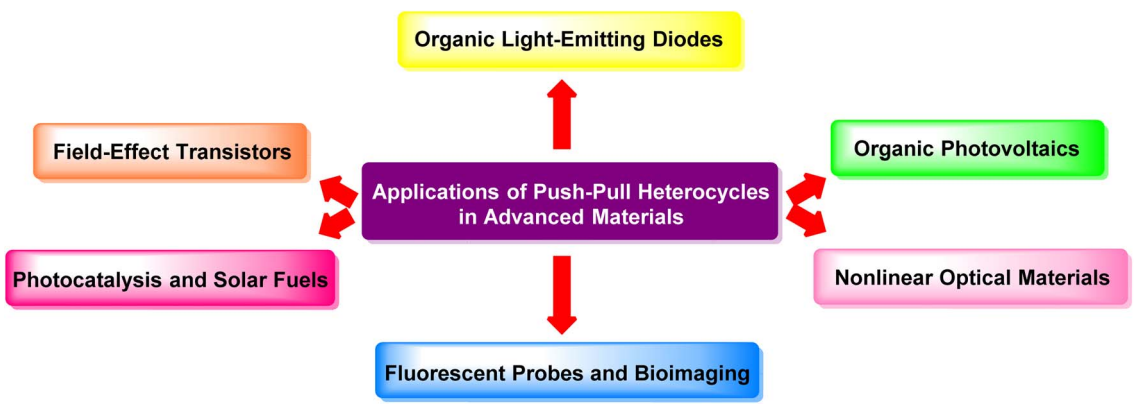

Fig. 6 Applications of push–pull heterocycles in advanced materials.

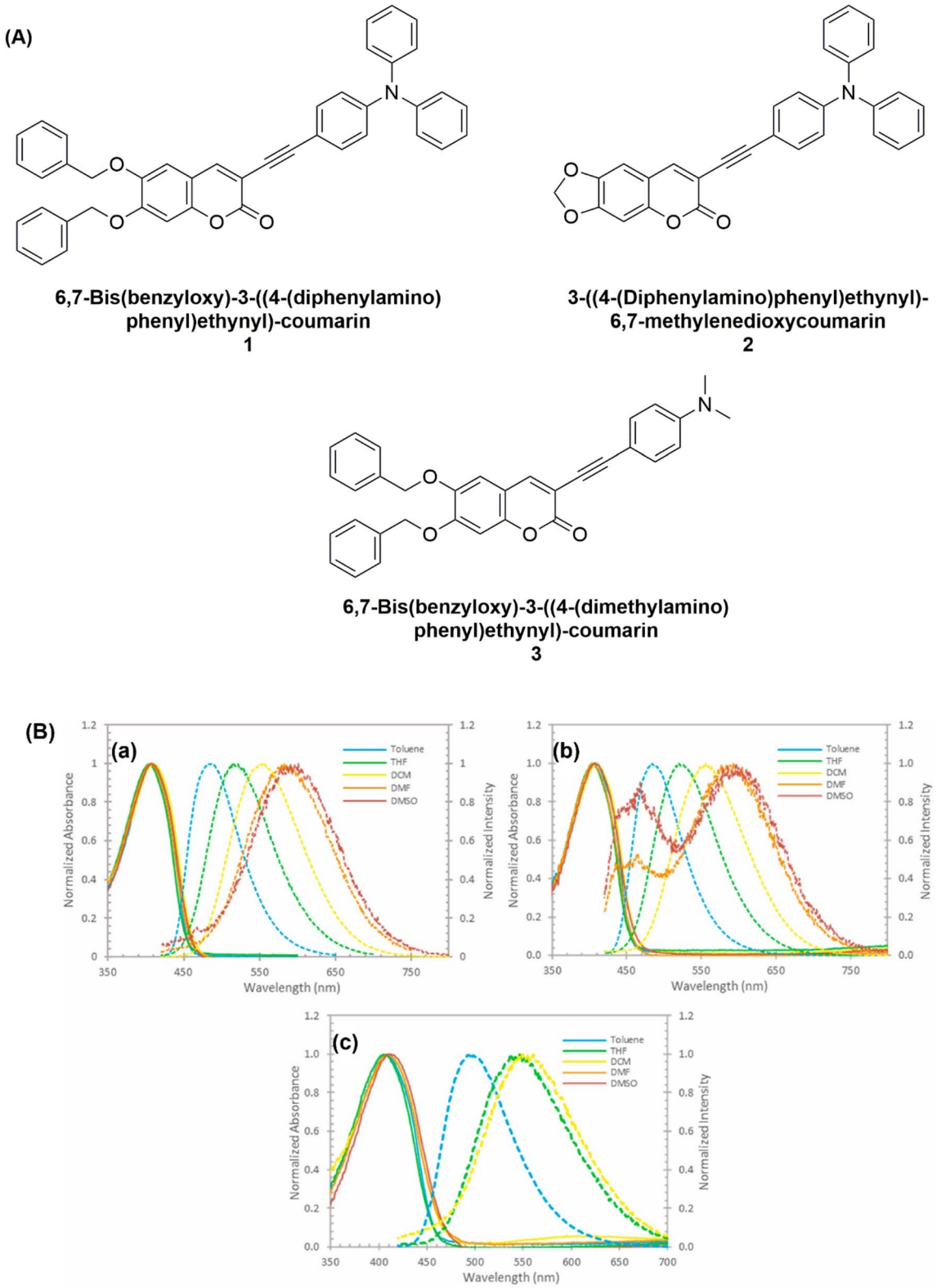

Fig. 7 (A) Chemical structure of coumarin dyes **1**, **2**, **3**. (B) Normalized absorption (solid lines) and fluorescence emission spectra (dashed lines) of coumarin derivatives (a) (top left), (b) (top right), and (c) (bottom) recorded in solvents of increasing polarity (toluene, DCM, THF, DMF, and DMSO). Reproduced from ref. 87 with permission from Elsevier, Copyright © 2024.

5.5 Photocatalysis and solar fuels

The photophysical attributes of push–pull heterocycles are advantageous for visible-light photocatalysis and water splitting: their broad absorption, redox tunability, and charge-separation efficiency enhance catalytic turnover. Metal-free photocatalysts based on D–π–A–π–D organic frameworks show excellent H_2 evolution performance under visible light.[84]

5.6. Organic field effect transistors (OFETs)

Some rigid push–pull systems also function as organic semiconductors in OFETs: highly planar, conjugated systems with strong π–π stacking improve charge carrier mobility. Acceptor-rich backbones improve electron-transporting capabilities for *n*-type OFETs.[85,86]

6 Recent advances in the photophysical properties of heterocyclic push–pull chromophores

Branco *et al.* (2024) reported the synthesis of three novel coumarin dyes (**1–3**) bearing an electron-donating (4-aminophenyl)ethynyl substituent at the 3-position of the scaffold (Fig. 7A). Despite exhibiting nearly identical absorption profiles ($\lambda_{abs} \approx 410$ nm), the dyes displayed distinct solvent-dependent emission behaviors. All compounds showed positive solvatochromism, with emission maxima progressively red-shifted and intensities reduced as solvent polarity increased. The normalized UV-vis absorption and emission spectra of the three coumarin derivatives were recorded in five solvents of

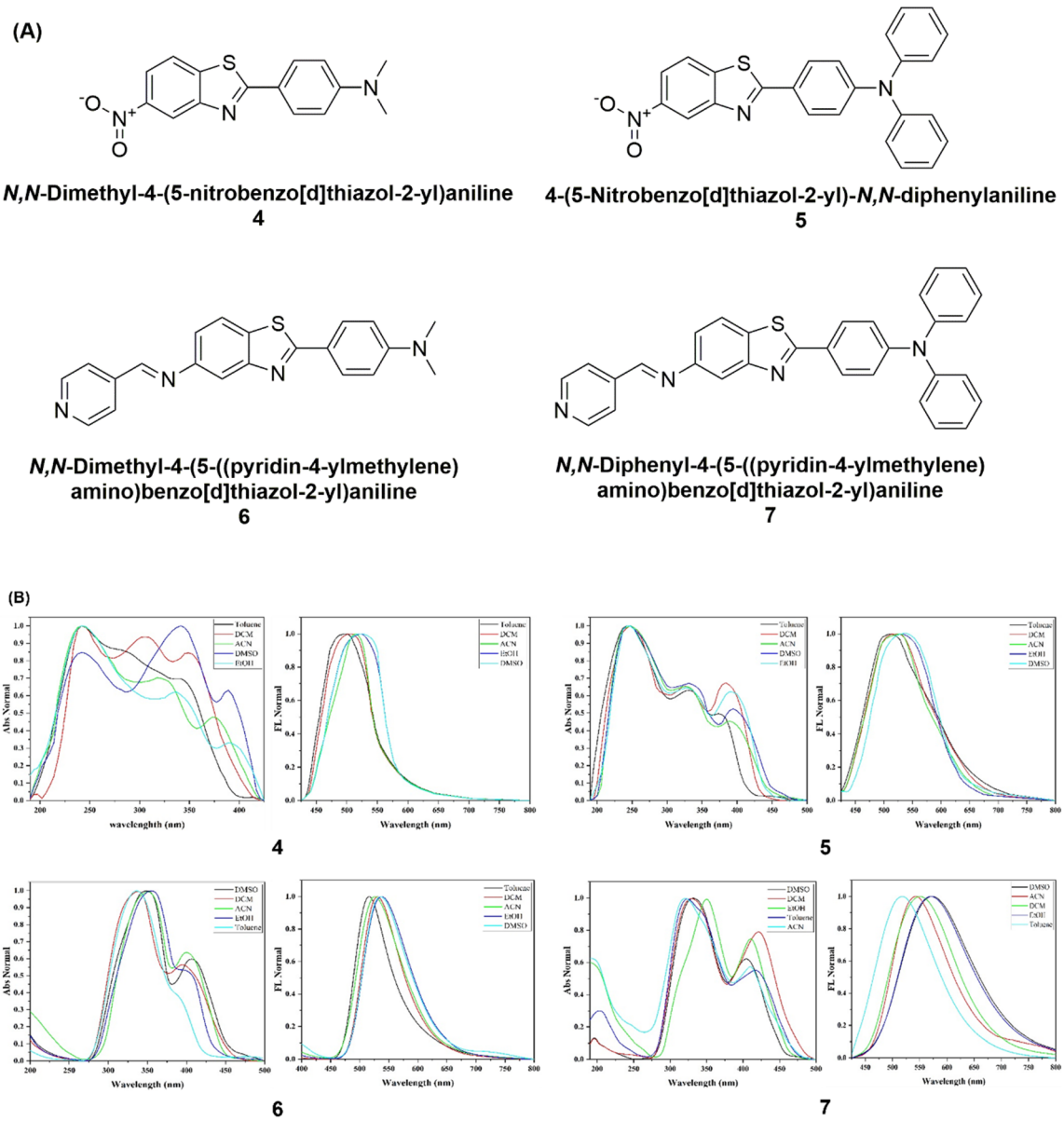

Fig. 8 (A) Chemical structure of benzothiazoles **4**, **5**, **6** and **7**. (B) Normalized absorption and emission spectra of synthesized conjugates (**4–7**) in different solvents. Reproduced from ref. 88 with permission from Elsevier, Copyright © 2024.

systematically increasing polarity: toluene, tetrahydrofuran (THF), dichloromethane (DCM), *N*,*N*-dimethylformamide (DMF), and dimethyl sulfoxide (DMSO), with $E_T(30)$ polarity parameters ranging from 0.10 to 0.44. While the absorption profiles remained nearly unchanged across solvents, centered around 410 nm, the emission spectra displayed a marked

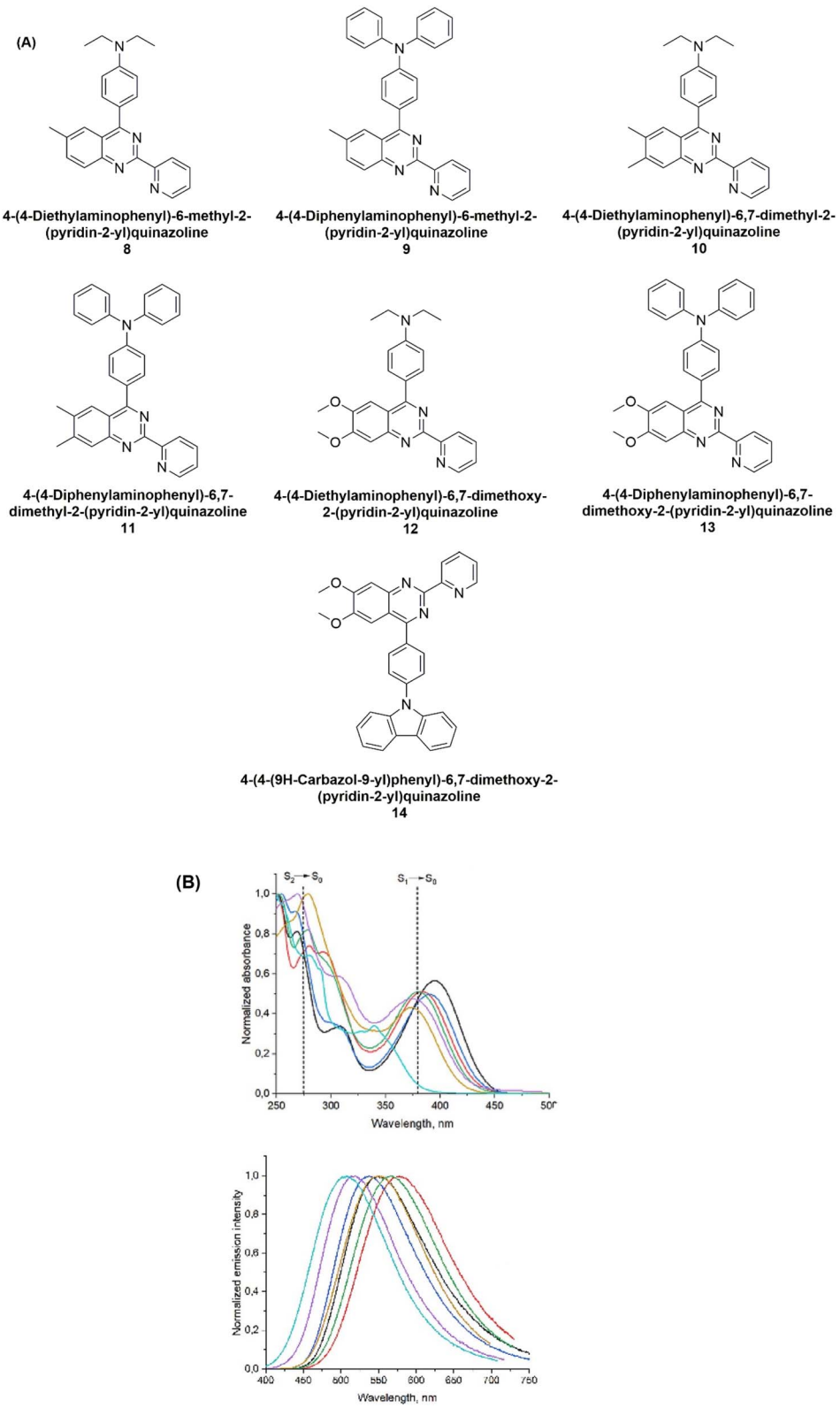

Fig. 9 (A) Chemical structure of quinazoline derivatives (**8–14**). (B) Normalized absorption (a) and emission (b) spectra of (**8–14**) in MeCN ($c = 1 \times 10^{-5}$ M, r.t.). Reproduced from ref. 89 with permission from Wiley, Copyright © 2024.

positive solvatochromic shift accompanied by decreasing fluorescence intensity as solvent polarity increased. The fluorescence profiles of A and B were comparable, with emission maxima spanning 480 nm (toluene) to 600 nm (DMSO). In contrast, coumarin C exhibited more pronounced red-shifted emission and complete quenching in polar solvents such as

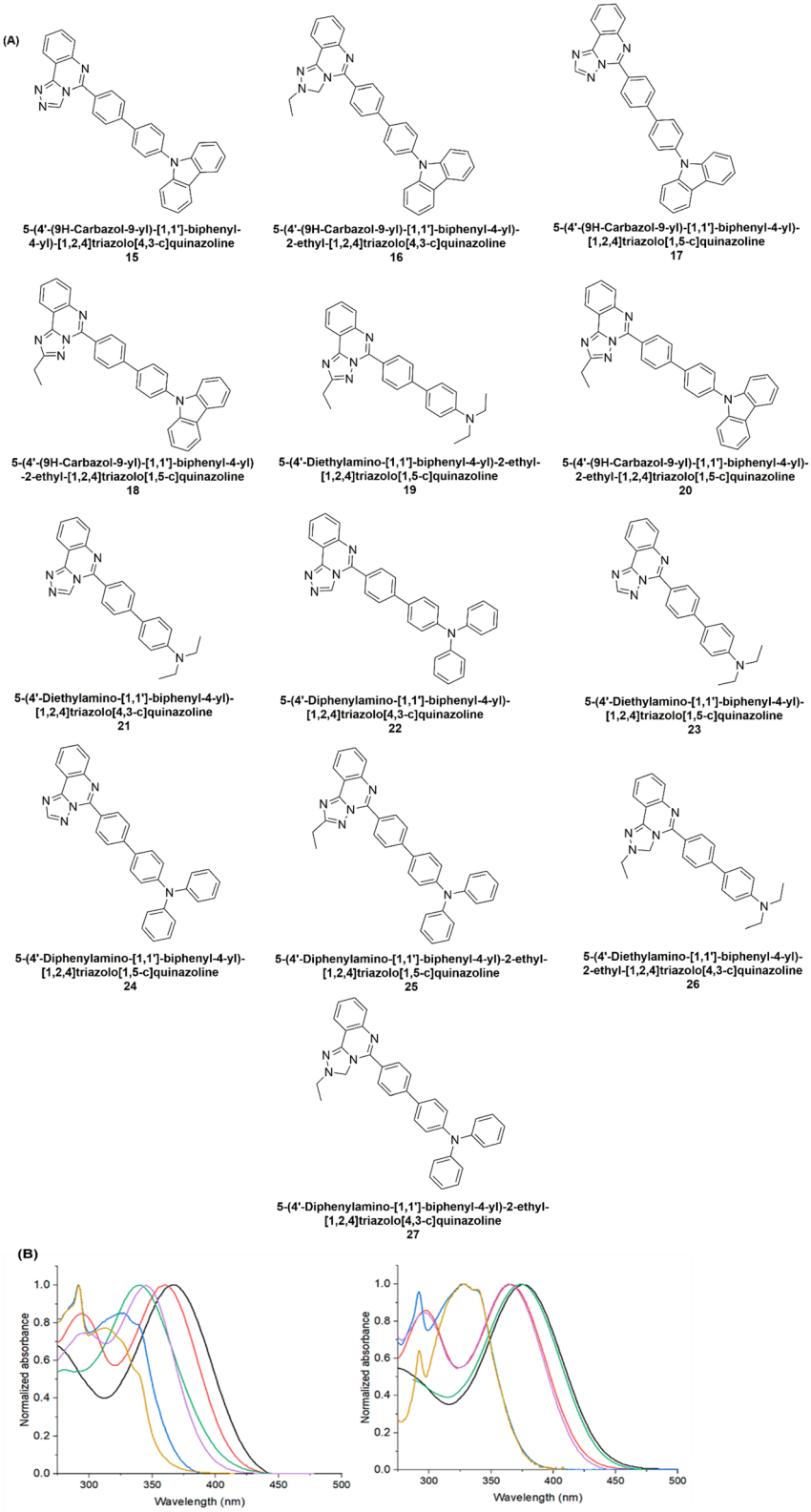

Fig. 10 (A) Chemical structure of compounds **15–27**. (B) Normalized absorption spectra of triazoloquinazolines in MeCN. Reproduced from ref. 90, under the terms of the CC BY 3.0 license.

DMF and DMSO, suggesting a stronger ICT process due to the enhanced electron-donating nature of the dimethylamino group relative to the diphenylamino moiety (Fig. 7B). The observed reduction in quantum yield in polar media was attributed to narrowing of the singlet–ground state energy gap, which facilitates non-radiative deactivation pathways in accordance with the energy-gap law.[87]

Zghab *et al.* (2024) synthesized four benzothiazole conjugates (**4–7**) and investigated their photophysical behavior in solvents of varying polarity (Fig. 8A). The absorption spectra showed solvent-dependent bathochromic shifts, with λ_{max} values of 337–389 nm (**4**), 373–394 nm (**5**), 387–417 nm (**6**), and 393–423 nm (**7**). DMSO consistently produced the highest absorption maxima, reflecting strong solute–solvent interactions in polar environments. Fluorescence studies revealed similar polarity effects. Conjugates **4** and **5** emitted at 495–522 nm and 512–531 nm, respectively, with ethanol showing the most intense fluorescence. Conjugates **6** and **7** emitted at 518–537 nm and 518–571 nm, with maxima observed in DMSO (**6**) and ethanol (**7**). Overall, increasing solvent polarity induced red-shifted emissions and intensity variations, indicating stabilization of the excited states. Stokes shift analysis further confirmed significant solvent reorganization, with higher values for **4** (6550–9472 cm^{-1}) and **5** (6732–7278 cm^{-1}), and moderate values for **6** (5916–6577 cm^{-1}) and **7** (4676–7239 cm^{-1}). The prominent absorption of **5** in DMSO (λ_{max} = 389 nm) is attributed to π–π* transitions enhanced by the nitro and diphenylamino substituents (Fig. 8B). These results emphasize the critical influence of solvent polarity on the electronic transitions and excited-state dynamics of the benzothiazole conjugates.[88]

Nosova *et al.* (2024) reported a series of 2-(2-pyridyl)quinazoline derivatives (**8–14**) bearing donor aryl substituents with methyl or methoxy groups (Fig. 9A). In acetonitrile (MeCN), all compounds displayed strong absorption bands at 250–325 nm (ε > 15 000 M^{-1} cm^{-1}) corresponding to $S_0 \rightarrow S_2$ transitions, alongside lower-energy bands around 340–380 nm (ε = 9700–12,100 M^{-1} cm^{-1}) assigned to $S_0 \rightarrow S_1$ transitions. The carbazolyl analogue **14** showed a hypsochromic shift compared to Et_2N and Ph_2N derivatives (**12**, **13**), attributed to weaker

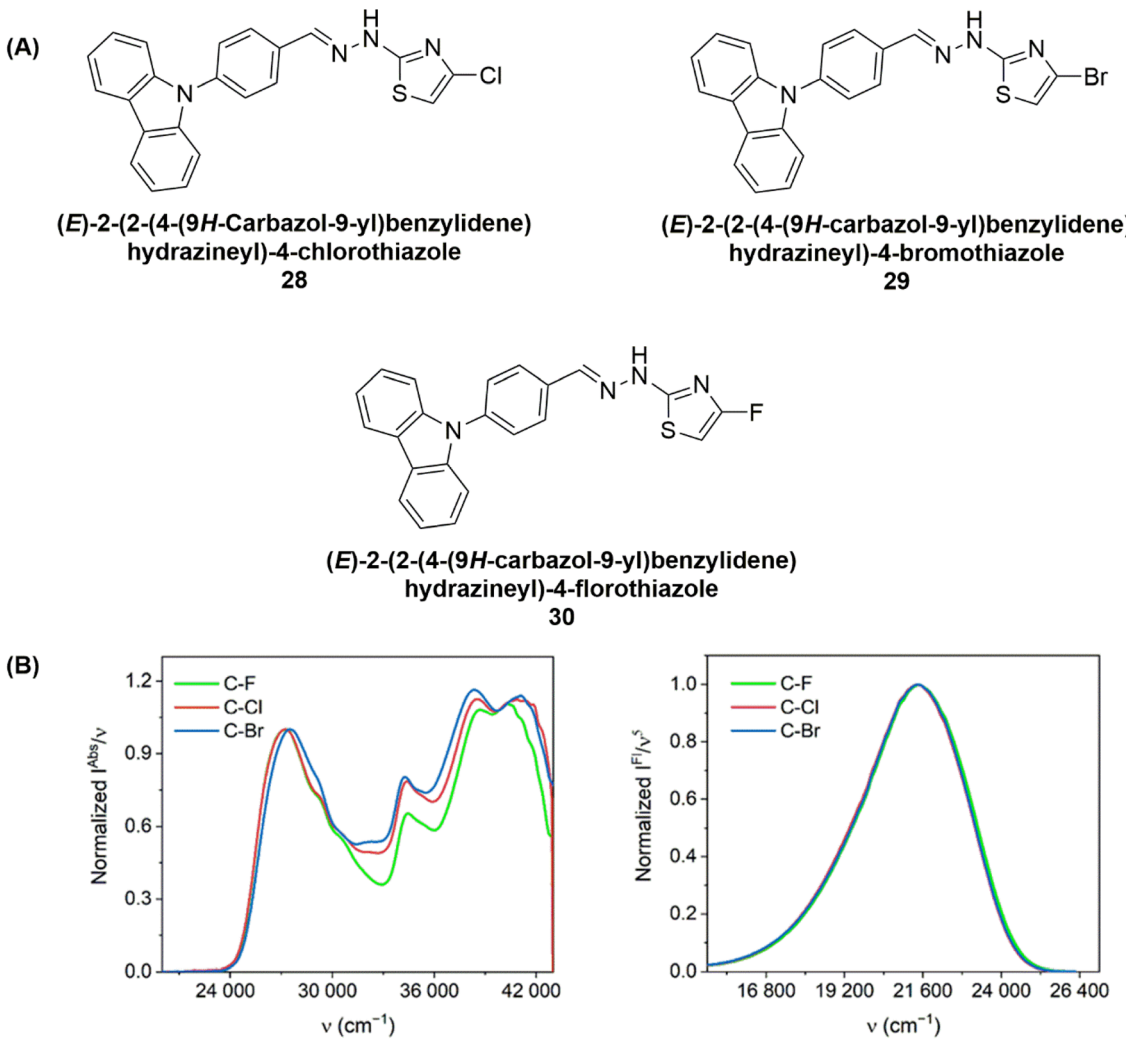

Fig. 11 (A) Chemical structure of carbazole–thiazole dyes **28–30**. (B) Normalized steady-state absorption (left) and fluorescence (right) spectra of the synthesized derivatives in $CHCl_3$ (λ_{ex} = 366 nm). Reproduced from ref. 91 under the terms of the CC BY 3.0 license.

conjugation of the rigid carbazole unit. A systematic blue shift in absorption and emission was observed from methyl → dimethyl → dimethoxy substitution, reflecting enhanced electron-donating effects. The emission profiles of compounds (**8–14**) in MeCN (Fig. 9B) reveal fluorescence ranging from the green to orange region. Among them, **9** [4-(4-diphenylamino) phenylquinazoline with a methyl group at C-6] displays the most red-shifted emission. Incorporation of an additional methyl group (6,7-dimethyl derivative **11**) or replacement of methyl substituents with methoxy groups (6,7-dimethoxy derivative **13**) induces a progressive blue shift in emission. Furthermore, substitution of the arylamino donor from

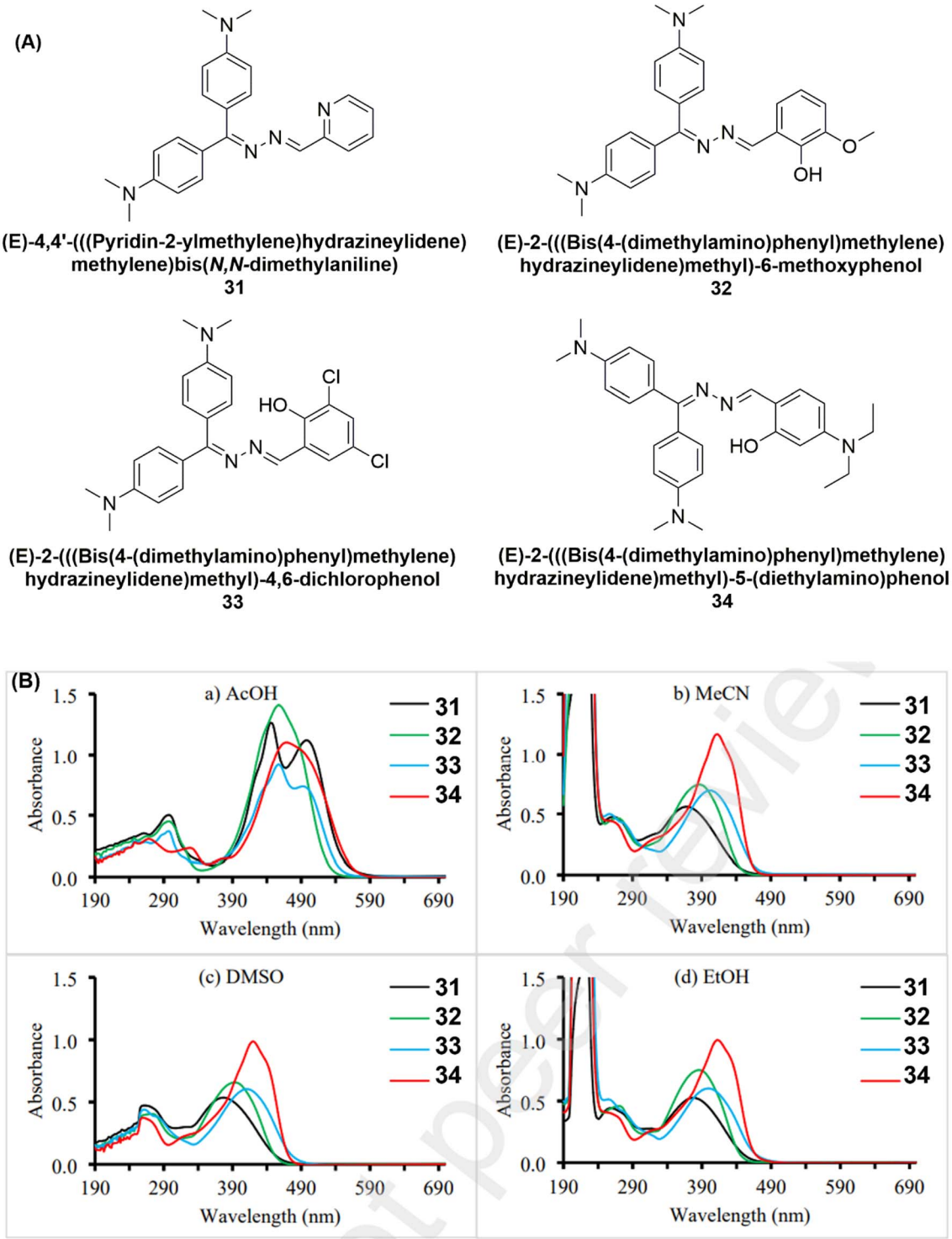

Fig. 12 (A) Chemical structure of azines **31–34**. (B) UV-vis absorption spectra of compounds **31–34** (1.7×10^{-5} M) recorded in AcOH (a), MeCN (b), DMSO (c), and EtOH (d).[92]

diphenylamino to diethylamino results in a hypsochromic shift of 26–34 nm, confirming the stronger donor capacity of the diphenylamino moiety within this system. These observations are consistent with previously reported trends for related 2,4-disubstituted quinazolines. Quantum yield and solvent-dependent fluorescence studies revealed TICT-state stabilization in polar media for Et_2N/Ph_2N analogues, while carbazolyl derivatives favored PLICT emission. Two-photon absorption reached up to 210 GM in toluene, with methoxy substitution lowering cross-sections. Henceforth, these results highlight 2-(2-pyridyl)quinazolines as promising push–pull luminophores for optoelectronic and bioimaging applications.[89]

Nosova *et al.* (2024) reported a versatile approach for synthesizing 5-(4-bromophenyl)-[1,2,4]triazolo[4,3-*c*]quinazolines and their [1,5-*c*] isomers (**15–27**), followed by a detailed investigation of their photophysical behavior in solution and solid state (Fig. 10A). The absorption maxima of carbazolyl-containing derivatives were observed at 312–328 nm in MeCN, while their Et_2N- and Ph_2N-substituted analogues displayed red-shifted bands in the 340–375 nm region, with slightly longer

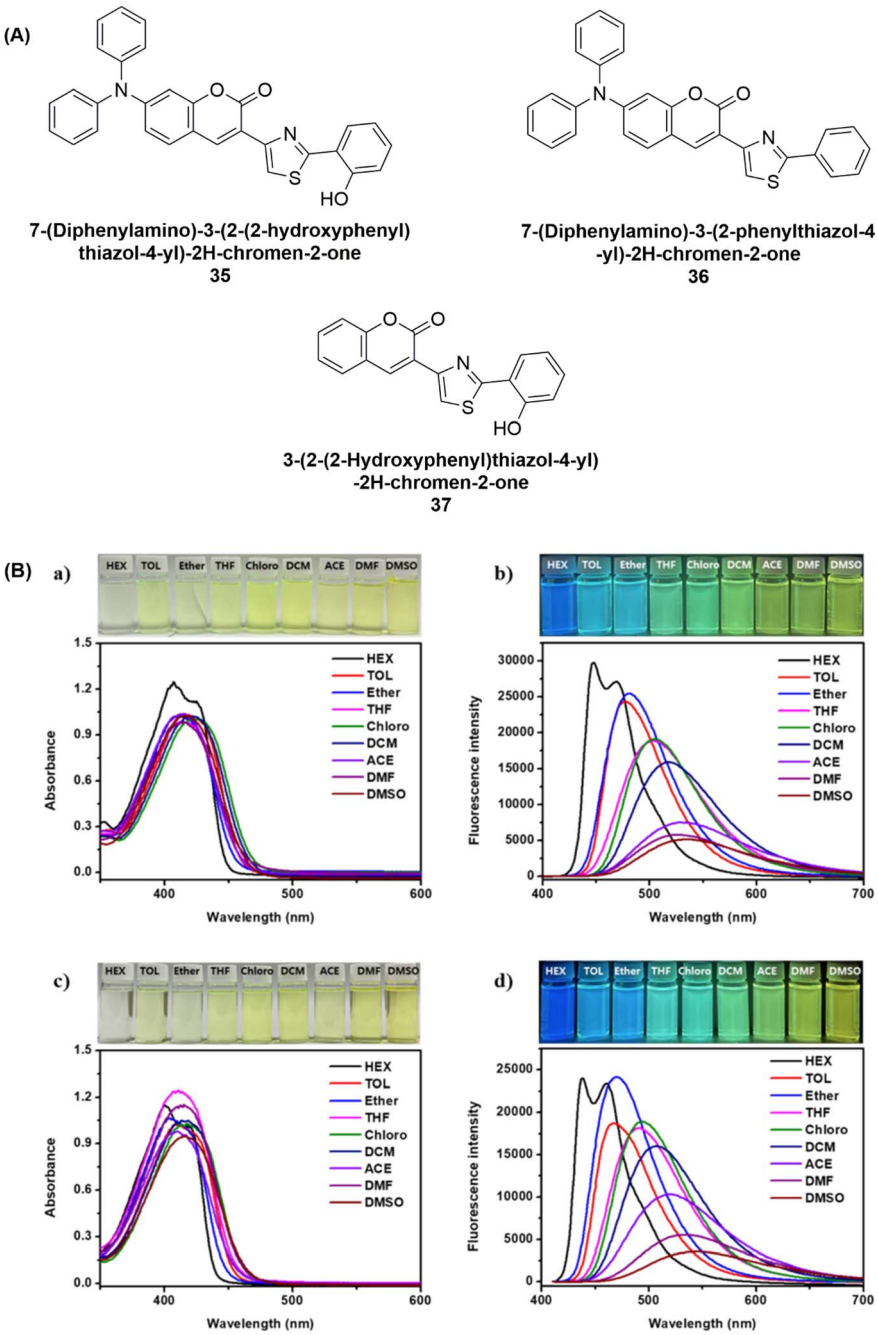

Fig. 13 (A) Chemical structure of compounds **35–37**. (B) Solution photographs and corresponding spectra of **35** and **36** (2.5×10^{-5} M): (a) compound **35** under daylight with absorption spectrum, (b) compound **35** under UV light with fluorescence spectrum, (c) compound **36** under daylight with absorption spectrum, and (d) compound **36** under UV light with fluorescence spectrum.[93]

wavelengths in toluene. Emission studies revealed strong fluorosolvatochromism, with blue–cyan emission in toluene shifting to yellow–orange in MeCN. Remarkably, [1,5-*c*] isomers exhibited higher fluorescence efficiency, with quantum yields exceeding 75% in toluene. The absorption characteristics were strongly influenced by the aminoaryl substituent. Carbazolyl derivatives (**15**, **16**, **17**, **18**) showed consistent absorption at 312–328 nm, whereas Et_2N- and Ph_2N derivatives absorbed at longer wavelengths (340–375 nm). In [4,3-*c*] triazoloquinazolines, the presence of an ethyl group induced a hypsochromic shift due to steric twisting of the biphenyl unit, while in [1,5-*c*] analogues this effect was negligible. Moreover, [1,5-*c*] annelation generally caused a bathochromic shift relative to [4,3-*c*] counterparts. All derivatives were emissive in both solvents with varying intensities. Et_2N- and Ph_2N-substituted compounds emitted at 465–486 nm in toluene, whereas carbazolyl derivatives showed blue–violet emission (420–441 nm). In MeCN, emission bands shifted markedly to lower energies, appearing at 530–548 nm for carbazolyl derivatives and 593–609 nm for their Et_2N-/Ph_2N analogues. Quantum yield analysis revealed three distinct groups: (i) highly emissive compounds ($\Phi_F \geq 90\%$) in both solvents (**19**, **20**), (ii) derivatives with high Φ_F only in toluene (**21**, **22**, **23**, **24**, **25**) and (iii) compounds showing solvent-dependent emission efficiency (**15**, **16**, **26**, **27**) (Fig. 10B). Henceforth, the synthesized push–pull systems display pronounced fluorosolvatochromism, arising from significant dipole moment changes upon excitation. Their intense emission in aprotic solvents highlights their potential as promising candidates for practical applications as fluorescence probes.[90]

Krawczyk *et al.* (2024) synthesized and evaluated three novel carbazole–thiazole derivatives bearing halogen substituents (Cl, Br, and F). Their absorption and steady-state fluorescence spectra were first examined in chloroform (Fig. 11A). All compounds display absorption bands with maxima at ~363–366 nm, characterized by high molar extinction coefficients (24 100–27,500 M^{-1} cm^{-1}), typical of $\pi \rightarrow \pi^*$ transitions. Additional weaker bands appear between 280–300 nm, corresponding to n $\rightarrow$ π^* transitions. The nearly identical absorption features across the series suggest that the halogen substituents at the *p*-position of the phenyl ring exert little influence on the $S_0 \rightarrow S_1$ transition. Fluorescence lifetimes and emission spectra were also recorded in chloroform (Fig. 11B). All derivatives exhibit emission centered at 454 nm. Substitution with halogens does not alter the emission maximum but affects intensity, with

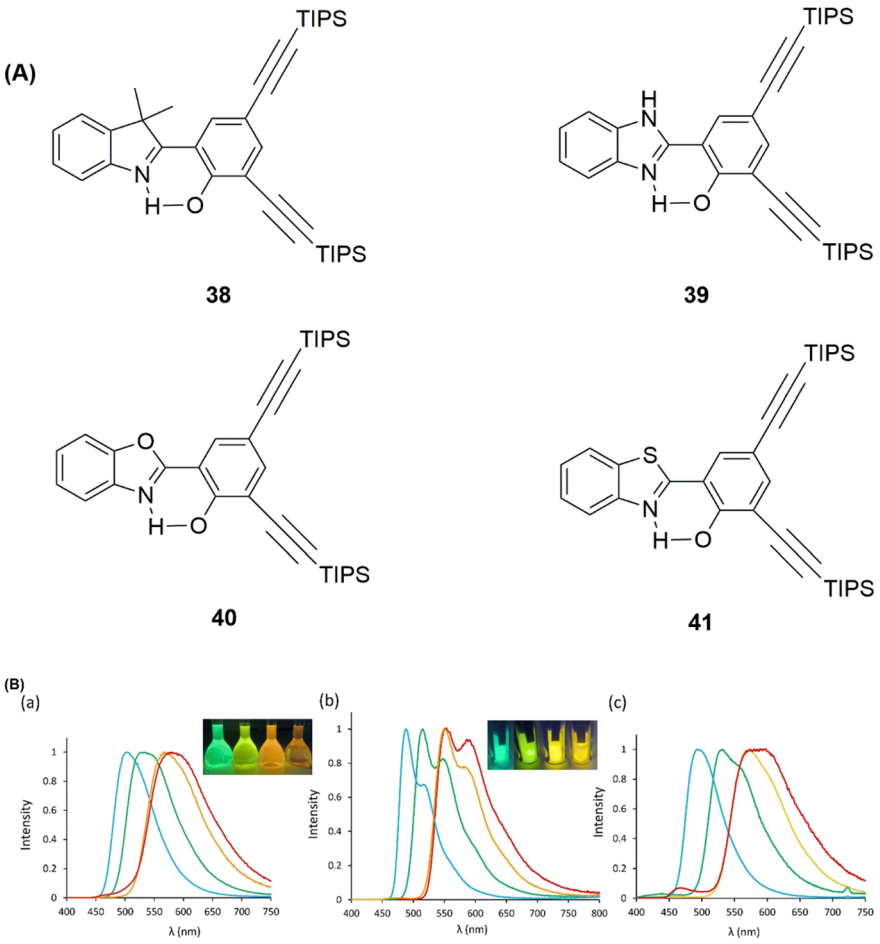

Fig. 14 (A) Chemical structure of dyes **38**–**41**. (B) Normalized emission spectra of **38** (red) **39** (blue), **40** (green), **41** (orange) measured in (a) CH_2Cl_2 at 25 °C, (b) MeTHF at 77 K (1 μM), and (c) in the solid state, embedded in 1 wt% KBr pellets. Reproduced from ref. 25 under the terms of the CC (BY-NC) 3.0 license.

fluorine-substitution giving the highest fluorescence yield (Φ_F = 11.37%), followed by chlorine (10.98%) and bromine (7.33%). The decrease in quantum yield for the heavier halogen analogues can be attributed to enhanced non-radiative decay pathways, particularly ISC facilitated by the heavy atom effect. In particular, the presence of bromine increases the likelihood of S → T transitions, resulting in faster ISC relative to fluorescence. These results demonstrate that the materials serve as efficient platforms for developing fully organic fluorescent probes.[91]

Shraim *et al.* (2024) synthesized four asymmetric azine derivatives (**31–34**) (Fig. 12A), containing Michler's ketone and either 2-pyridyl or salicyl units in high yields. Their UV-vis spectra (1.7×10^{-5} M) revealed two to three main absorption bands depending on solvent. In AcOH, **31**, **32**, **33** showed maxima near 297–298 nm, while **34** exhibited peaks at 269 and 328 nm. Visible bands varied: **31** and **33** presented dual absorptions (447/498 nm and 457/492 nm), whereas **32** and **34** showed overlapping maxima (458 and 469 nm). Similar patterns were observed in DMSO, with shifts to shorter wavelengths, while MeCN and EtOH produced three bands (222–229, 257–270, and 369–412 nm), attributable to n–σ*, π–π*, and n–π* transitions. Solvent effects revealed strong solvatochromism, particularly in AcOH, which induced redshifts with enhanced absorbance compared to MeCN, EtOH, and DMSO. Differences were linked to solvent polarity and protic/aprotic nature, as well as pK_a values. All derivatives displayed fluorescence, with **32** and **33** showing the highest intensity in AcOH. Compound **31** exhibited solvent-dependent emissions, *e.g.*, λ_{max} 362 nm in AcOH, 512 nm in MeCN, dual bands at 433/464 nm in EtOH, and an intense 520 nm band in DMSO. Emission generally decreased with concentration, except for one band in EtOH (Fig. 12B). Henceforth, compounds (**31–34**) demonstrate strong solvent-dependent absorption and fluorescence behavior, underscoring their potential in nonlinear optics, catalysis, and chemosensing applications.[92]

Son *et al.* (2024) synthesized new materials by incorporating electron-donating and electron-accepting groups onto a coumarin core. For comparison, two structurally related compounds were also prepared to evaluate their optical behavior and stability. In the case of **35** and **36**, absorption bands appear between 410–430 nm, corresponding to π–π* charge transfer transitions, whereas **37** exhibits its main absorption near 350 nm. As a result, **35** and **36** absorb in the visible region, accounting for their yellow coloration (Fig. 13A). Photophysical investigations in nine solvents of increasing polarity—hexane (HEX), toluene (TOL), diethyl ether (ether), tetrahydrofuran (THF), chloroform (chloro), dichloromethane

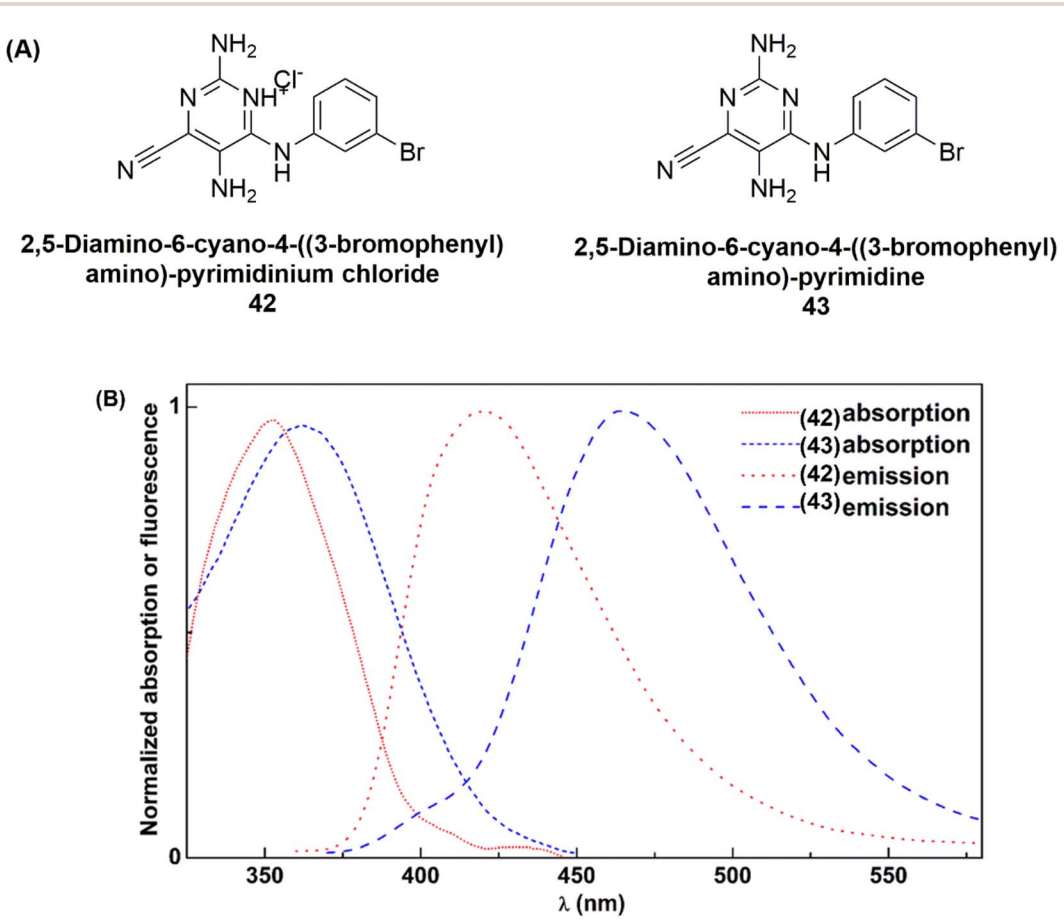

Fig. 15 (A) Chemical structure of compounds **42** and **43**. (B) Normalized UV-vis absorption and fluorescence spectra of compounds **42** and **43** (2.5×10^{-6} M) recorded in dioxane. Reproduced from ref. 94 under the terms of the CC (BY-NC) 3.0 license.

(DCM), acetone (ACE), dimethylformamide (DMF), and dimethyl sulfoxide (DMSO)—revealed that higher solvent polarity leads to reduced fluorescence intensity and a red shift of approximately 100 nm relative to non-polar solvents (Fig. 13B). These solvatochromic effects are strongly influenced by the presence of hydroxyl groups, which engage in hydrogen bonding due to the electronegativity of oxygen, and by triphenylamine, which acts as an electron donor. The interplay of donor and acceptor substituents modulates ICT, with electron-rich groups generally inducing a red shift in both absorption and emission spectra.[93]

Massue *et al.* (2024) reported a novel class of ESIPT-based fluorophores derived from the well-established 2-(2′-hydroxyphenyl)benzazole (HBX) scaffold (Fig. 14A). By linking 3,3′-dimethylindole (or 3*H*-indole) units with phenolic rings, they developed new 2-(2′-hydroxyphenyl)-3,3′-dimethylindole (HDMI) derivatives capable of exhibiting stimuli-responsive ESIPT fluorescence. These compounds show red-shifted emission compared to HBX and demonstrate unique acid/base-dependent stabilization of distinct rotamers, facilitated by supramolecular interactions involving methyl substituents. The bis-ethynyl-extended derivative **38** was synthesized to explore the photophysical behavior of the HDMI scaffold. In dichloromethane, **38** showed a red-shifted absorption maximum at 382 nm compared with HBX analogues (362–373 nm) and emitted at 580 nm, also red-shifted relative to HBX **39–41** (504–566 nm). Although its quantum yield (0.04) increased four-fold over the parent compound, it remained weak compared with HBX derivatives, likely due to the influence of the CMe_2 group promoting non-radiative decay. Low-temperature measurements (MeTHF, 77 K) revealed a pronounced blue shift (490–555 nm) and enhanced emission, particularly for **38**, attributed to restricted molecular motions. In the solid state, compounds **38–41** displayed strong fluorescence with emission spanning 495–583 nm and improved quantum yields (0.09–0.46) (Fig. 14B).[25]

Dias *et al.* (2024) reported a new series of 2,4,5-triaminopyrimidine derivatives and evaluated their photophysical properties (Fig. 15A). For compounds **42** and **43**, absorption maxima, emission maxima, molar absorption coefficients, fluorescence quantum yields, and Stokes shifts were systematically determined. The molar absorption coefficients, generally ranging between 1–2.5 × 10^4 M^{-1} cm^{-1}, indicate allowed electronic transitions from the ground to excited states. Both compounds exhibit low fluorescence quantum yields in protic solvents due to solute–solvent hydrogen bonding, while significantly higher efficiencies are observed in non-protic solvents. Comparative studies between neutral and protonated species revealed that the neutral forms display enhanced emission yields in non-protic media such as dichloromethane and dioxane, but reduced efficiencies in protic environments like aqueous buffer, highlighting their potential in microenvironment sensing. When compared to previously reported fluorescent pyrimidine analogues, which absorb at 290–330 nm and emit at 374–430 nm, these newly synthesized derivatives demonstrate red-shifted optical features, with absorption centered near 360 nm, emission around 470 nm, and notably large Stokes shifts (83 nm in aqueous buffer and 108 nm in dioxane). Furthermore, they exhibit remarkably high fluorescence quantum yields (Φ_F = 0.5–0.6 in dioxane) and substantial brightness ($\varepsilon \cdot \Phi_F \approx 15\,000$ M^{-1} cm^{-1}). This performance greatly surpasses earlier pyrimidine analogues, whose brightness values were limited to 2000–3800 M^{-1} cm^{-1} (Fig. 15B). The study concludes that the newly synthesized 2,4,5-triaminopyrimidine derivatives exhibit strong photophysical properties, including red-shifted absorption/emission, large Stokes shifts, and high fluorescence quantum yields, making them promising candidates for fluorescent probe applications.[94]

Shkoor *et al.* (2025) reported the synthesis and photophysical characterization of 3,3′-sulfonylbis(7-(diethylamino)-2*H*-chromen-2-one), a highly efficient fluorescent push–pull system

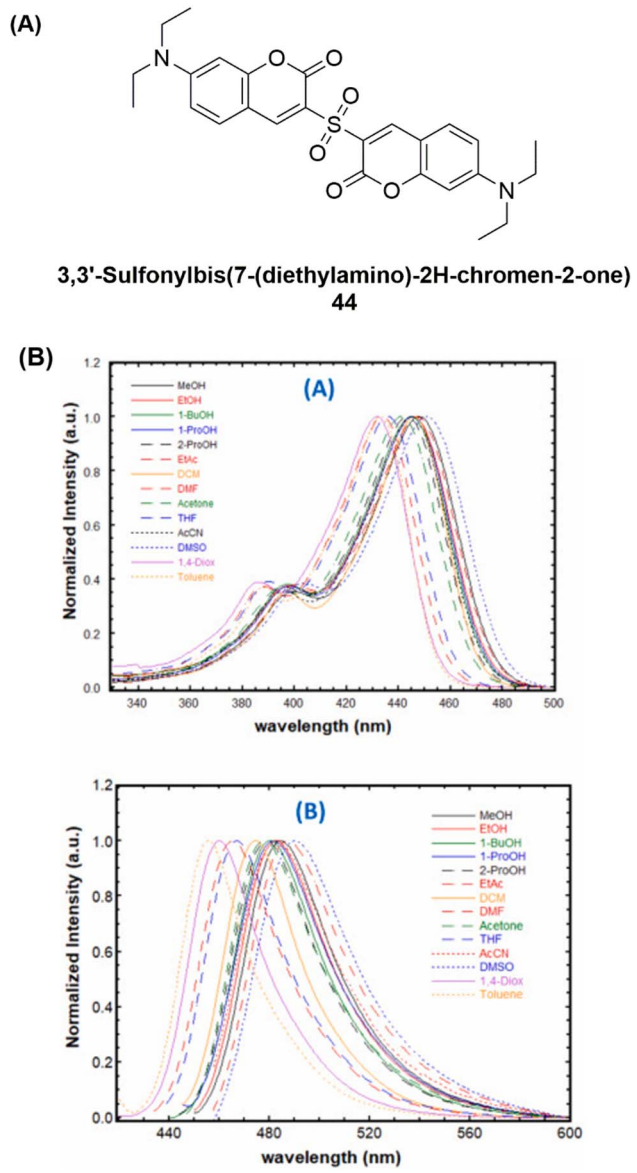

Fig. 16 (A) Chemical structure of bis-coumarinyl sulfone **44**. (B) Absorption (A) and emission (B) spectra of bis-coumarinyl sulfone recorded in various neat solvents. Reproduced from ref. 95 with permission from Elsevier, Copyright © 2025.

with a donor–π–acceptor–π–donor (D–π–A–π–D) framework (Fig. 16A). This molecular architecture exhibited pronounced solvatochromism, strongly influenced by the surrounding medium. Absorption and fluorescence spectra were recorded in solvents of varying polarity, revealing significant bathochromic shifts with increasing solvent polarity. Moreover, fluorescence quantum yields varied noticeably across solvents, with the highest efficiencies observed in nonpolar media. The UV-vis absorption spectrum of the bis-coumarinyl sulfone in neat solvents displayed a broad absorption band at 448 nm, accompanied by a shoulder near 400 nm. These bands provide valuable insights into the electronic transitions and conjugation within the system. The strong absorption at 448 nm corresponds to a π–π* transition, supported by high molar extinction coefficients ($\varepsilon = 2.8 \times 10^4 - 3.6 \times 10^4$ M^{-1} cm^{-1}), confirming the highly allowed nature of this transition in the extended conjugated scaffold. The additional shoulder around 400 nm is likely attributed to a secondary transition, vibronic structure, or solvent/substituent interactions involving the diethylamino groups on the coumarin core (Fig. 16B). The fluorescence spectrum revealed an emission maximum at 485 nm, corresponding to a substantial Stokes shift of ~18 500 cm^{-1}. This large shift highlights efficient energy dissipation through internal conversion and vibrational relaxation prior to photon emission, consistent with the behavior of strongly conjugated push–pull chromophores. This study establishes a solid

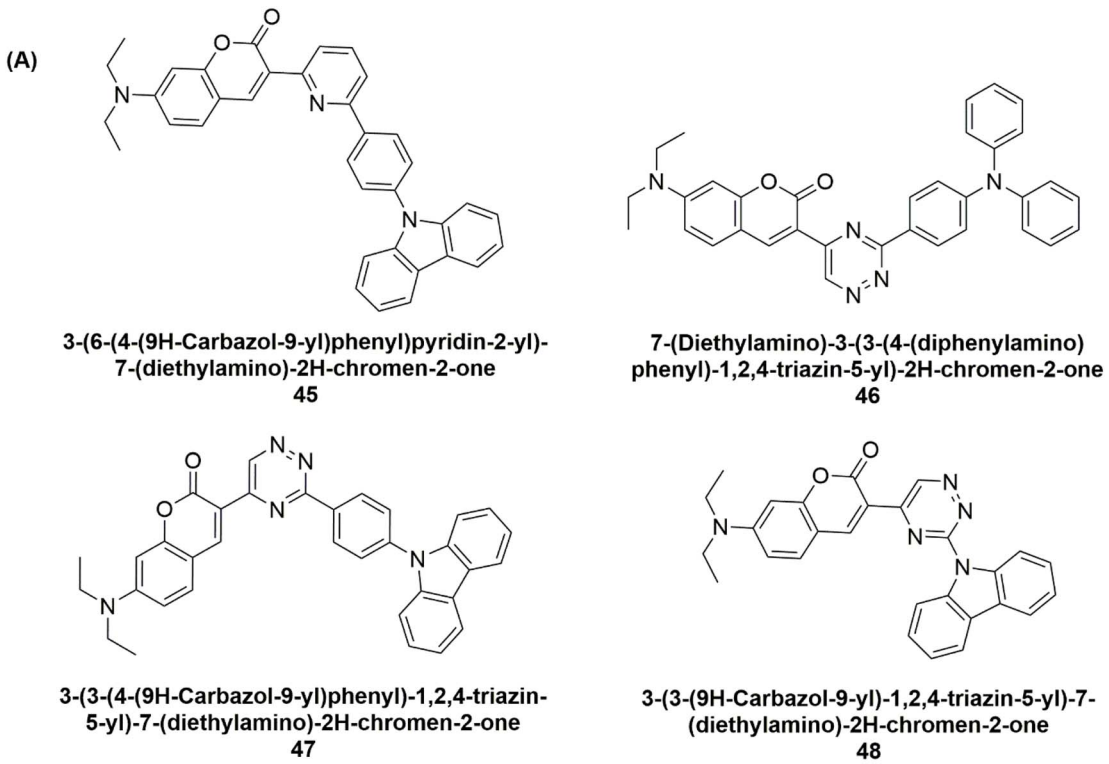

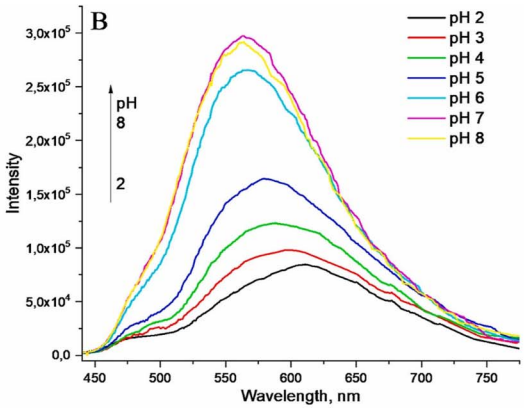

Fig. 17 (A) Chemical structure of coumarins **45–48**. (B) Emission spectra of compound **45** ($c = 1.0 \times 10^{-5}$ M) in BRB/DMSO (99 : 1, v/v) solution over the pH range 2–8. Reproduced from ref. 96 with permission from Elsevier, Copyright © 2025.

foundation for the rational development of advanced fluorescent materials with tunable photophysical properties, enabling their potential use in sensing, bioimaging, and optoelectronic technologies.[95]

Fatykhov *et al.* (2025) synthesized and investigated a series of 3-triazinyl- and 3-pyridinyl-substituted coumarin dyes (Fig. 17A) for their linear and NLO properties, along with charge-transfer behavior. The triazine-based fluorophores exhibited green emission, while the pyridine analogues displayed blue emission, both with high fluorescence quantum yields. Two-photon fluorescence measurements revealed that compound **45** possessed a notable two-photon absorption cross-section (δ_{2PA} = 285.5 GM). Additionally, these dyes demonstrated significant second-order NLO activity, with static hyperpolarizability (β_0) values ranging from 43 to 78 × 10^{-30} esu. Solvatochromic studies, supported by calculated charge-transfer (CT) indices, confirmed the occurrence of ICT processes and demonstrated a clear dependence of CT intensity on structural variations within the triazine derivatives, following the order: **46** > **47** > **48**. The compounds exhibited strong absorption in the $S_0 \rightarrow S_1$ transition, with high molar extinction coefficients (ε_M up to 2.28 × 10^5 M^{-1} cm^{-1} at λ_{max}, abs > 400 nm) (Fig. 17B). Their pronounced sensitivity to solvent polarity, along with notable pH responsiveness within the biologically relevant range, suggests that these fluorophores are highly suitable as fluorescent probes for cellular imaging applications.[96]

Dengiz *et al.* (2025) reported the design of push–pull chromophores exhibiting pronounced ICT, which results in strong ground-state polarization and enhanced NLO responses. The ICT efficiency, and consequently the NLO activity, was found to be strongly dependent on the donor and acceptor strength of the substituents. Two distinct classes of NLO phores were synthesized *via* [2 + 2] cycloaddition–retroelectrocyclization reactions of heteroaryl-substituted electron-rich alkynes with tetracyanoethylene (TCNE) and tetracyanoquinodimethane (TCNQ). The resulting chromophores (**49**, **50**) displayed charge-transfer absorption bands with λ_{max} spanning 424–758 nm. Their linear and NLO properties were systematically investigated using both experimental and computational approaches. NLO measurements performed with a validated custom-built Z-scan setup revealed nonlinear absorption coefficients ranging from −1.44 × 10^{-4} to −9.90 × 10^{-4} cm W^{-1}, along with nonlinear refractive indices between −1.59 × 10^{-7} and −2.26 × 10^{-6} cm^2 W^{-1} (Fig. 18). These findings suggest that the synthesized compounds possess strong potential for NLO applications.[97]

Zhang *et al.* (2025) synthesized three indolo[3,2-*b*]carbazole derivatives functionalized with β-diketone boron difluoride groups (ICZ-H, ICZ-F, and ICZ-CH_3) (**51–53**) (Fig. 19A). Their photophysical characteristics were systematically investigated in both organic solvents and aggregated states, with a detailed analysis of structure–property relationships. UV-vis absorption and fluorescence spectra across different solvents revealed intense absorption bands around 490 nm, with maximum molar extinction coefficients exceeding 6.0 × 10^4 L mol^{-1} cm^{-1}. Fluorescence intensity decreased with increasing solvent polarity, accompanied by red-shifts in emission maxima. In mixed tetrahydrofuran–water systems, the aggregation-induced fluorescence behavior showed an initial decrease followed by recovery in emission intensity, indicating preservation of fluorescence during aggregation. In the solid state, all derivatives exhibited emission above 630 nm, characteristic of red fluorescence (Fig. 19B). This offers a fundamental framework for the rational design of high-performance organic red fluorescent materials.[98]

Erdemir *et al.* (2025) reported the synthesis of tetraarylpyrrolo1[3,2-*b*]pyrroles (TAPP) derivatives bearing various substituents on the *N*-phenyl rings *via* a high-yielding one-pot procedure. Compounds (**54–56**) (Fig. 20A) were further functionalized at the 3,6-positions of the pyrrolopyrrole core through a Vilsmeier–Haack formylation, affording novel A–D–A type pyrrolopyrrole systems (**57–59**). The photophysical behavior of these derivatives was systematically examined in different solvents. Compounds (**54–56**) displayed absorption

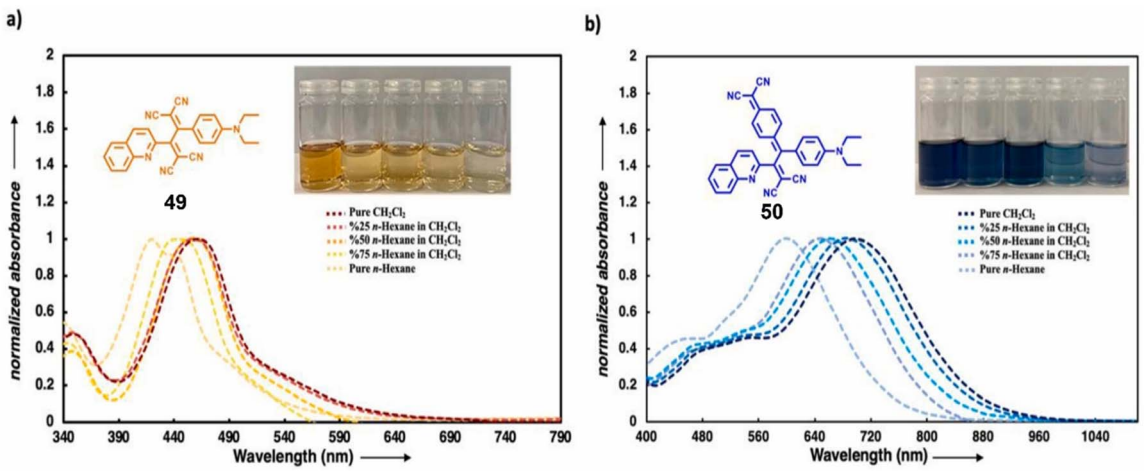

Fig. 18 UV-vis absorption spectra of compounds (a) **49** and (b) **50** recorded in *n*-hexane/CH_2Cl_2 mixtures at 298 K. Reproduced from ref. 97 with permission from Elsevier, Copyright © 2025.

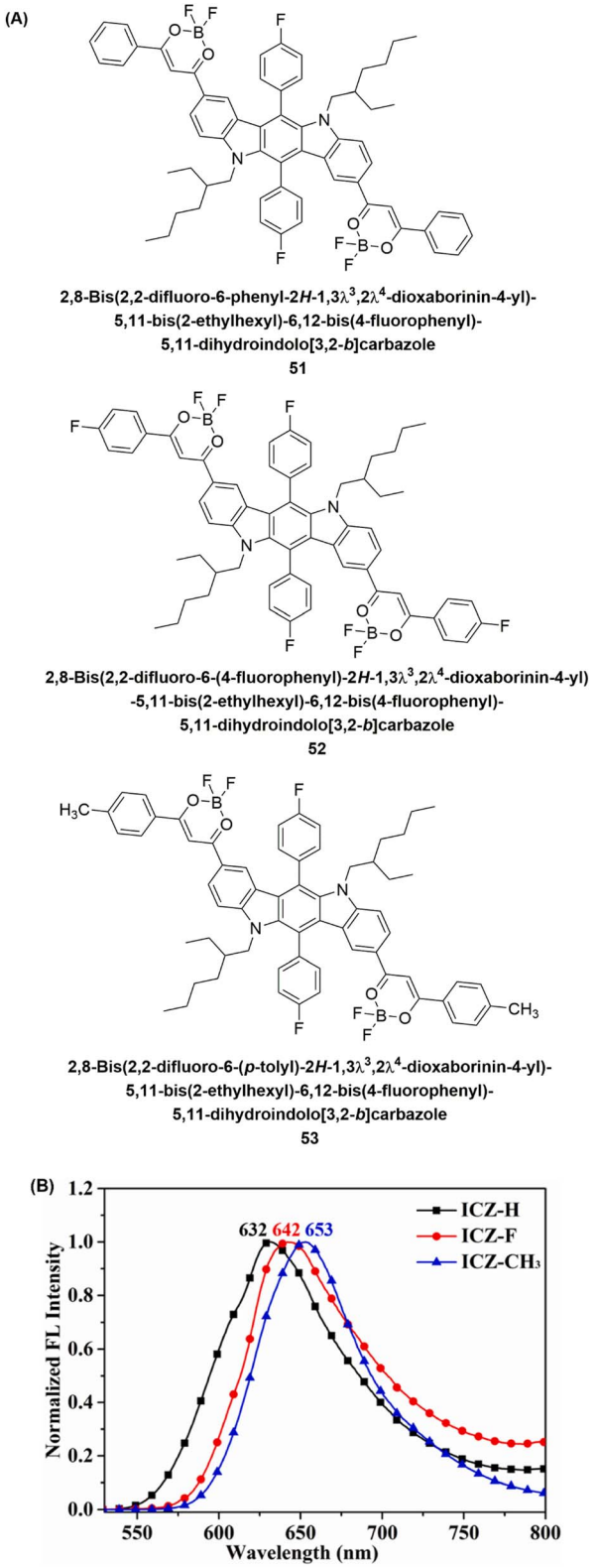

Fig. 19 (A) Chemical structure of carbazole derivatives **51–53**. (B) Fluorescence emission spectra of the three indolo[3,2-*b*]carbazole derivatives. Reproduced from ref. 98 with permission from Elsevier, Copyright © 2025.

maxima near 400 nm and fluorescence emission around 450 nm. For compounds **55** and **58**, the absorption maxima were observed at 400 nm and 350 nm, respectively, with corresponding emission peaks at 455 nm and 440 nm. Introduction of electron-withdrawing formyl groups at the 3,6-positions induced the formation of an A–D–A framework, resulting in a pronounced Stokes shift and a notable hypsochromic shift (~50 nm) in the absorption spectra. This phenomenon arises from the strong electron-withdrawing nature of the aldehyde substituents, which reduces the overall electron density of the molecule and consequently increases the energy of the π–π* transitions (Fig. 20B). The observed hypsochromic shift reflects absorption of higher-energy photons, enabling the molecule to interact efficiently with shorter-wavelength light. Such behavior enhances light sensitivity and wavelength selectivity, making these systems particularly promising for optoelectronic and photonic applications.[99]

Thippeswamy *et al.* (2025) examined the photophysical characteristics of deep-blue fluorescent 5-phenyl-4-tosyloxazole (**60**) through combined experimental and theoretical approaches (Fig. 21A). The absorption and fluorescence spectra of **60** were measured in a range of solvents, revealing that the Stokes shift displayed bathochromic behavior attributed to π → π* electronic transitions. A noticeable red shift in fluorescence maxima was observed with increasing solvent polarity. Upon excitation from the ground state (S_0) to the first excited state (S_1), both absorption (λ_a) and emission (λ_f) wavelengths varied depending on the solvent environment, reflecting differences in the stabilization and polarity of these states. In non-polar solvents such as hexane, pentane, and heptane, the absorption maxima appeared at shorter wavelengths (higher energy), consistent with limited stabilization of the excited state. The relatively small difference between ν_a and ν_f in these media suggested comparable stabilization of the ground and excited states. In contrast, in polar solvents such as DMSO, DMF, and ethanol, both absorption and emission maxima shifted to longer wavelengths (lower energy), indicating enhanced stabilization of the excited state by solvent polarity. The larger Stokes shift observed under these conditions demonstrated that the excited state possesses greater polarity than the ground state, resulting in stronger solvent–solute interactions and pronounced solvatochromic effects (Fig. 21B).[100]

Singh *et al.* (2025) investigated the photophysical properties of indolyl–coumarin hybrids **61–64** synthesized through green methods (Fig. 22A). Among twelve derivatives, compound **61** exhibited the highest fluorescence intensity, attributed to the synergistic donor–acceptor effects of methoxy (–OMe) and chloro (–Cl) substituents, which enhanced charge transfer and emission efficiency. In contrast, compound **62**, bearing a nitro group ($-NO_2$), showed complete fluorescence quenching due to its strong electron-withdrawing nature and promotion of non-radiative charge-transfer states. Several hybrids, particularly **63** and **64**, displayed typical AIE, with enhanced luminescence in water compared to DMSO (Fig. 22B). These findings highlight indolyl–coumarin hybrids as promising scaffolds for multifunctional fluorescent materials, with potential applications in bioimaging and optoelectronic devices.[101]

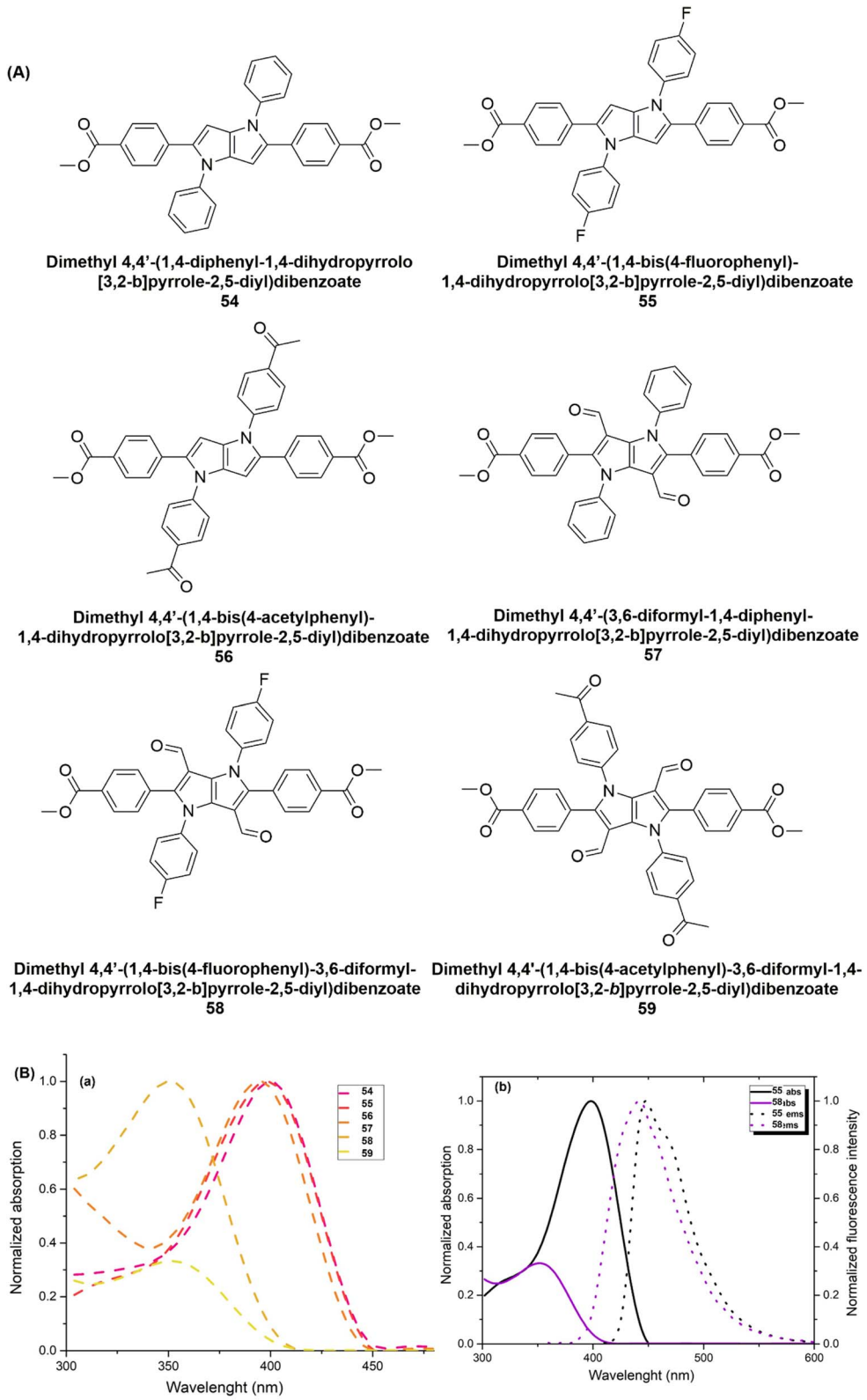

Fig. 20 (A) Chemical structure of pyrrole derivatives **54–59**. (B) (a) UV-vis spectra of derivatives **54–59**, (b) normalized absorption spectra (solid lines) and fluorescence emission spectra (dotted lines) of compounds **55** and **58**. Reproduced from ref. 99 with permission from Springer, Copyright © 2025 under the terms of the CC (BY-NC) 3.0 license.

Sangwan *et al.* (2025) reported the microwave-assisted synthesis of 4,6-diaryl-substituted 3-cyano-2-pyridones bearing various electron-donating and electron-withdrawing groups within a π-conjugated framework. All derivatives displayed absorption bands in the range of 362–389 nm, while their fluorescence emissions appeared between 431–454 nm. The

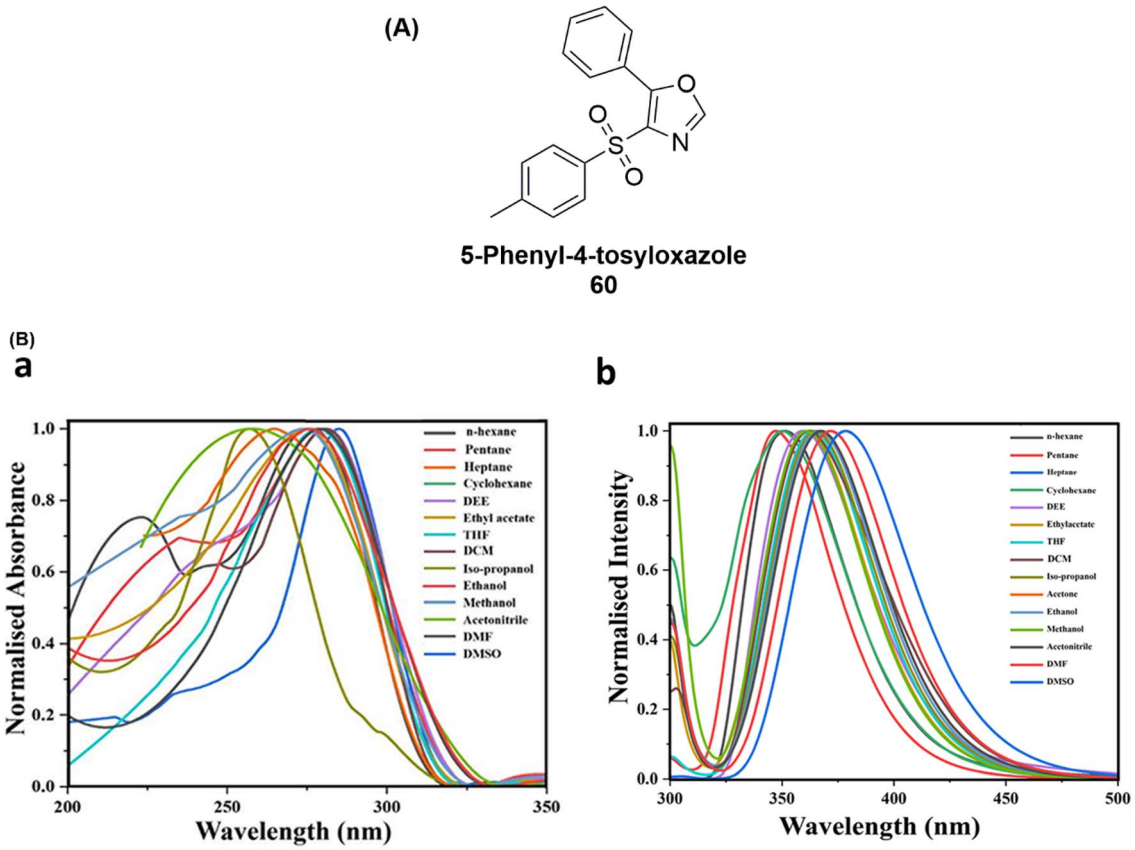

Fig. 21 (A) Chemical structure of compound **60**. (B) (a) Normalized absorption spectra of **60** in different solvents. (b) Normalized fluorescence spectra of **60** in different solvents.[100]

influence of solvent polarity on their optical behavior was systematically examined. For instance, compound **65** (Fig. 23A) exhibited absorption maxima within 280–400 nm, which shifted bathochromically by approximately 27 nm when moving from non-polar to polar solvents. In polar media such as DMF, DMSO, and water, the absorption maxima showed a less intense red shift, likely arising from ground-state hydrogen-bonding interactions with solvent molecules. Correspondingly, emission spectra recorded in the same solvent systems revealed maxima in the 431–454 nm region (Fig. 23B).[102]

Michinobu *et al.* (2025) synthesized a new series of 1,1,4,4-tetracyanobuta-1,3-diene (TCBD) derivatives incorporating different heterocyclic units, such as pyridine, carbazole, indole, and benzothiadiazole, *via* a [2 + 2] cycloaddition–retro-electrocyclization (CA–RE) reaction. These TCBD-based chromophores exhibited narrow band gaps, primarily attributed to strong intramolecular charge-transfer (ICT) interactions within the donor–acceptor framework. The UV-vis absorption spectra of compounds **67–70** were measured in CH_2Cl_2 solutions (5×10^{-5} M) at room temperature (Fig. 26A and B). Distinct ICT absorption bands were observed at 496.5 nm for **67**, 489.0 nm for **68**, 475.5 nm for **69**, and 576.5 nm for **70**. The optical band gaps, estimated from the absorption onsets, were 2.14, 2.02, 2.34, and 1.78 eV for **67–70**, respectively (Fig. 24). Particularly, for compound **69**, the ICT band underwent a further bathochromic shift with a marked increase in absorption intensity upon [2 + 2] CA–RE transformation.[103]

Kubo *et al.* (2025) reported the synthesis of highly annulated boron-dipyrromethene (BODIPY) derivatives aimed at developing NIR absorbing photodetectors. Among them, 3,5-diareno-BODIPY **71** exhibited the most red-shifted absorption, with a maximum at 680 nm ($\varepsilon = 1.27 \times 10^5$ M^{-1} cm^{-1}) and a weaker vibronic feature around 625 nm in THF (Fig. 25A). Incorporation of a thiophene unit in dye **72** induced a further 13 nm bathochromic shift relative to compound **71**. Upon excitation at 350 nm, strong NIR fluorescence was observed at 704 nm for **71** and 734 nm for **72**, with quantum yields (Φ) of 36% and 14%, respectively. Minimal solvent-dependent shifts were detected in both absorption and emission spectra (Fig. 25B), consistent with a typical π–π^* transition as supported by the Lippert–Mataga correlation. Remarkably, compound **72** showed a larger Stokes shift ($\Delta_s = 797$ cm^{-1}) compared to the thiophene-free analogue **71**, likely due to increased conformational flexibility of the thiophene ring. Further structural modification of compound **72** through intramolecular B,O-chelation produced the benzo[1,3,2]oxazaborinine-based dye **73**, which displayed a strong absorption band at $\lambda_{max} = 812$ nm ($\varepsilon = 1.3 \times 105$ M^{-1} cm^{-1}), consistent with results obtained from TD-DFT/DFT calculations. Interestingly, dye 14 showed dual-emission behavior upon excitation at 375 nm, giving bands at 822 nm

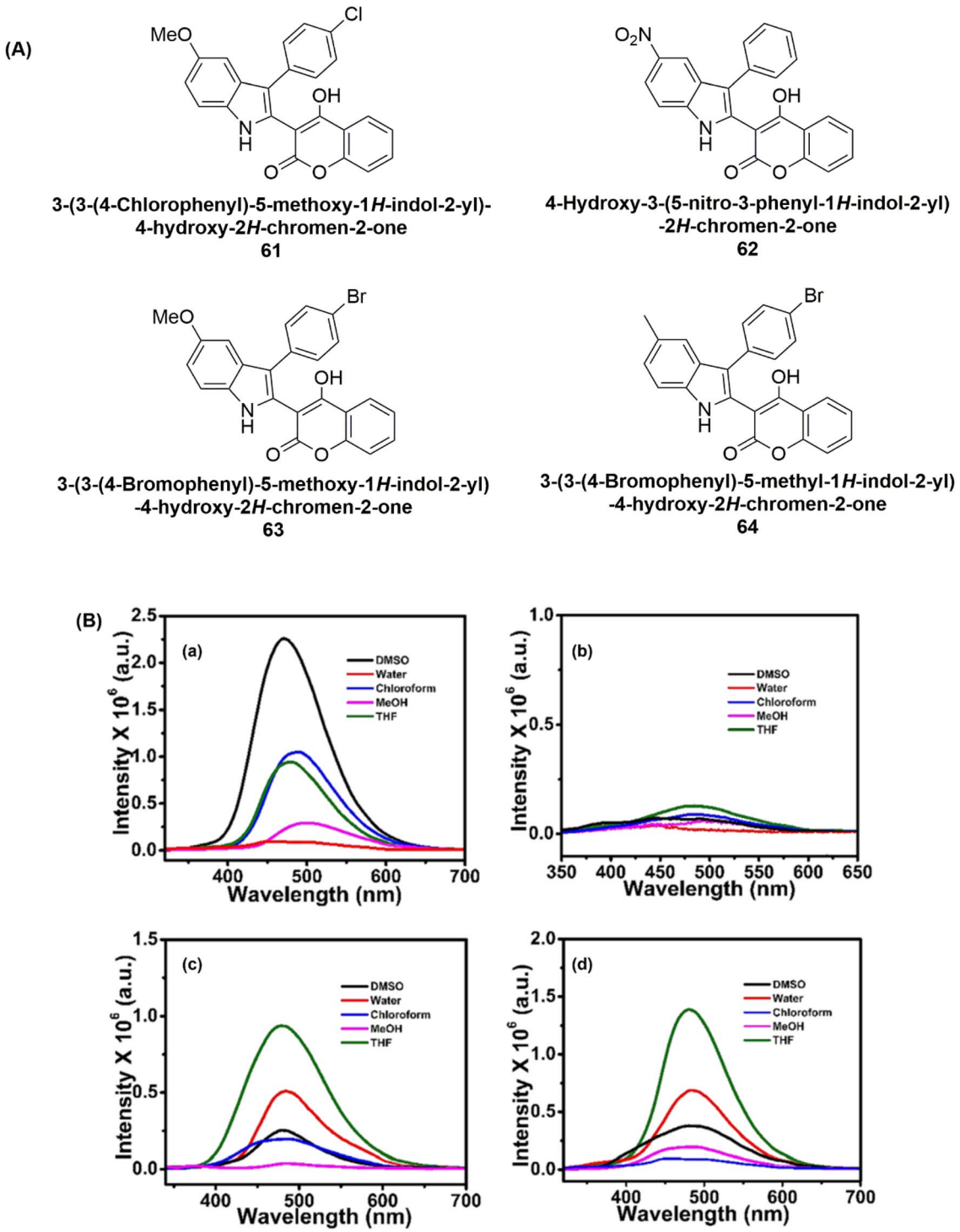

Fig. 22 (A) Chemical structure of indole coumarin derivatives **61**–**64**. (B) Normalized emission spectra of (a) **61**, (b) **62**, (c) **63**, (d) **64**. Reproduced from ref. 101 with permission from Wiley, Copyright © 2025.

($\Phi = 5.1\%$) and 470 nm ($\Phi = 7.8\%$). Given their robust thermal stability, particularly of compound **73**, these BODIPY systems demonstrate strong potential for application in NIR photodetectors for image-based sensing technologies.[104]

Achelle *et al.* (2025) reported the design and synthesis of a new series of push–pull fluorophores incorporating quinazoline-based acceptors. The molecular framework consisted of quinazoline cores substituted either with phenyl or methoxy groups, combined with electron-donating fragments such as 9,9-dimethylacridan (DMAC), phenoxazine (PXZ), or phenothiazine-T-Ph (**76**) (PTZ). To bridge the donor and acceptor moieties, either a 1,4-phenylene or 2,5-thienylene

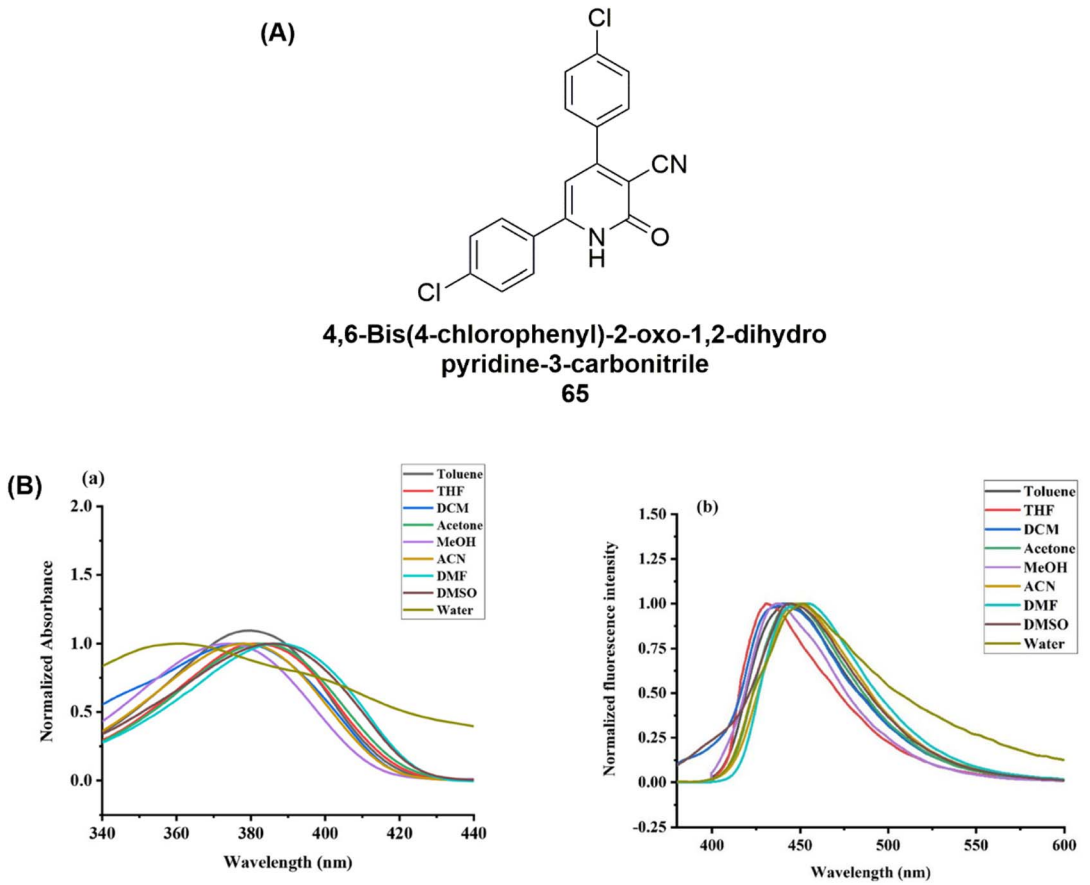

Fig. 23 (A) Chemical structure of pyridone **65**. (B) (a) Normalized UV-vis absorption spectrum of the compound **65** recorded in solvents of varying polarity. (b) Normalized fluorescence emission spectrum measured in the 400–600 nm wavelength range. Reproduced from ref. 102 with permission from Wiley, Copyright © 2025.

linker was introduced (Fig. 26A). The photophysical investigation revealed that all dyes exhibited prompt, short-lived fluorescence in solution. Spectroscopically, all derivatives displayed a distinct absorption band between 340 and 400 nm, largely unaffected by solvent polarity, with molar extinction coefficients ranging from 1600 to 8500 M^{-1} cm^{-1}. Additional absorption features were observed below 300 nm. Within the quinazoline framework, introduction of a thienylene linker or replacement of the phenyl substituent with a methoxy group led to a hypsochromic shift, as observed in DMAC-T-Ph (**75**) compared to DMAC-Ph (**74**) (Fig. 26B). Remarkably, for DMAC-Ph and PTZ-T-Ph, the lowest singlet transition ($S_1 \rightarrow S_0$) in the QE conformer acquired hybrid local and charge-transfer (HLCT) character, producing moderate oscillator strengths in agreement with the experimentally observed prompt fluorescence.[105]

López *et al.* (2025) synthesized a series of 6-aryl-2,4-bis(2′-hydroxyphenyl)pyrimidines was through efficient Suzuki–Miyaura coupling reactions and confirming their role as rigid tridentate O^N^O chelating ligands suitable for the preparation of four-coordinate organoboron complexes (Fig. 27A). In their free form, these ligands are non-emissive in both solution and the solid state. This behavior arises from intramolecular hydrogen bonding, which facilitates ESIPT process. The resulting excited keto tautomer undergoes rapid non-radiative decay, effectively quenching fluorescence. Interestingly, protonation or coordination with boron suppresses the ESIPT pathway, thereby restoring emissive properties. Furthermore, the emission can be systematically tuned by altering substituents on the aryl group. The optical characteristics of selected derivatives (**77a–e** and **78a–e**) were investigated using UV-vis absorption and fluorescence spectroscopy in dichloromethane at ambient temperature, as well as in the solid state (Fig. 27B). Ligands **77a–d** displayed comparable absorption features, with a dominant $\pi \rightarrow \pi^*$ transition band at 343–348 nm (**78a**). In contrast, the diphenylamino-substituted derivative **77e** exhibited a pronounced ICT character, reflected in a red-shifted absorption maximum at 405 nm due to the strong electron-donating nature of the amino group. Collectively, these findings highlight boron complexation as a powerful approach for tailoring the luminescent behavior of such pyrimidine-based ligands, underscoring their potential in optoelectronic applications and fluorescence-based sensing technologies.[106]

Navarro *et al.* (2025) the synthesis and comprehensive photophysical as well as computational characterization of a series of push–pull boron complexes, in which sterically demanding donor units are conjugated to a pyrimidine-based O^N^O boron

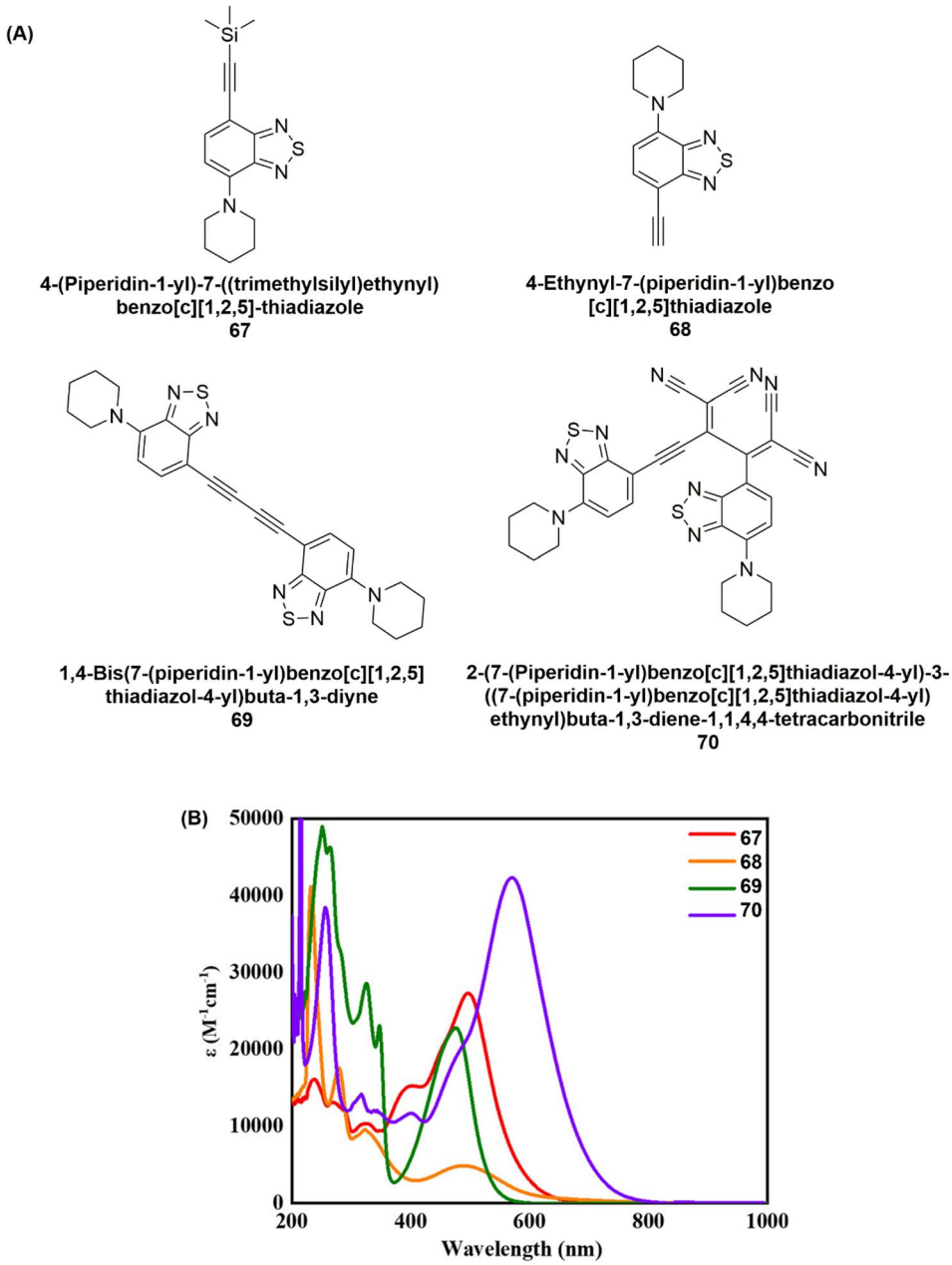

Fig. 24 (A) Chemical structure of TCBD derivatives **67–70**. (B) UV-vis absorption spectra of TCBD derivatives **67–70** recorded in CH_2Cl_2 solution (5×10^{-5} M) at room temperature. Reproduced from ref. 103 with permission from ACS Chemical Society, Copyright © 2025.

chelate (Fig. 28A). Among the investigated derivatives (**79a–c**), the dimethylacridan-substituted complex emerged as the most emissive, both in toluene solution and in the solid state (powder form). In deoxygenated media, this fluorophore displayed TADF, enabled by its small singlet–triplet energy gap. This observation parallels previously described pyridine analogues, which also demonstrated delayed emission behavior. The photophysical characteristics of boron fluoride complexes **79a–c** were systematically studied in toluene and in the solid state as amorphous powders (Fig. 28B). In solution, all complexes exhibited low-energy absorption features spanning 392–460 nm. Complexes **79b** and **79c** showed absorption maxima near 400 nm, while the phenoxazine-based analogue **79a** displayed a red-shifted band centered at 460 nm, in agreement with related structures (Fig. 28B(a)).[26] Upon excitation, complexes **79a** and **79c** produced single emission bands at 680 and 600 nm, respectively, whereas **79b** exhibited dual emission at 468 and 702 nm. The latter behavior is attributed to the coexistence of quasi-equatorial and quasi-axial conformers, a typical property of phenothiazine derivatives. Fluorescence quenching was pronounced in solution for complexes **79a** and **79b**; however, the dimethylacridan-containing complex **79c** demonstrated a markedly higher photoluminescence quantum yield ($\Phi_F = 0.24$), accompanied by a blue-shifted emission (λ_{em}

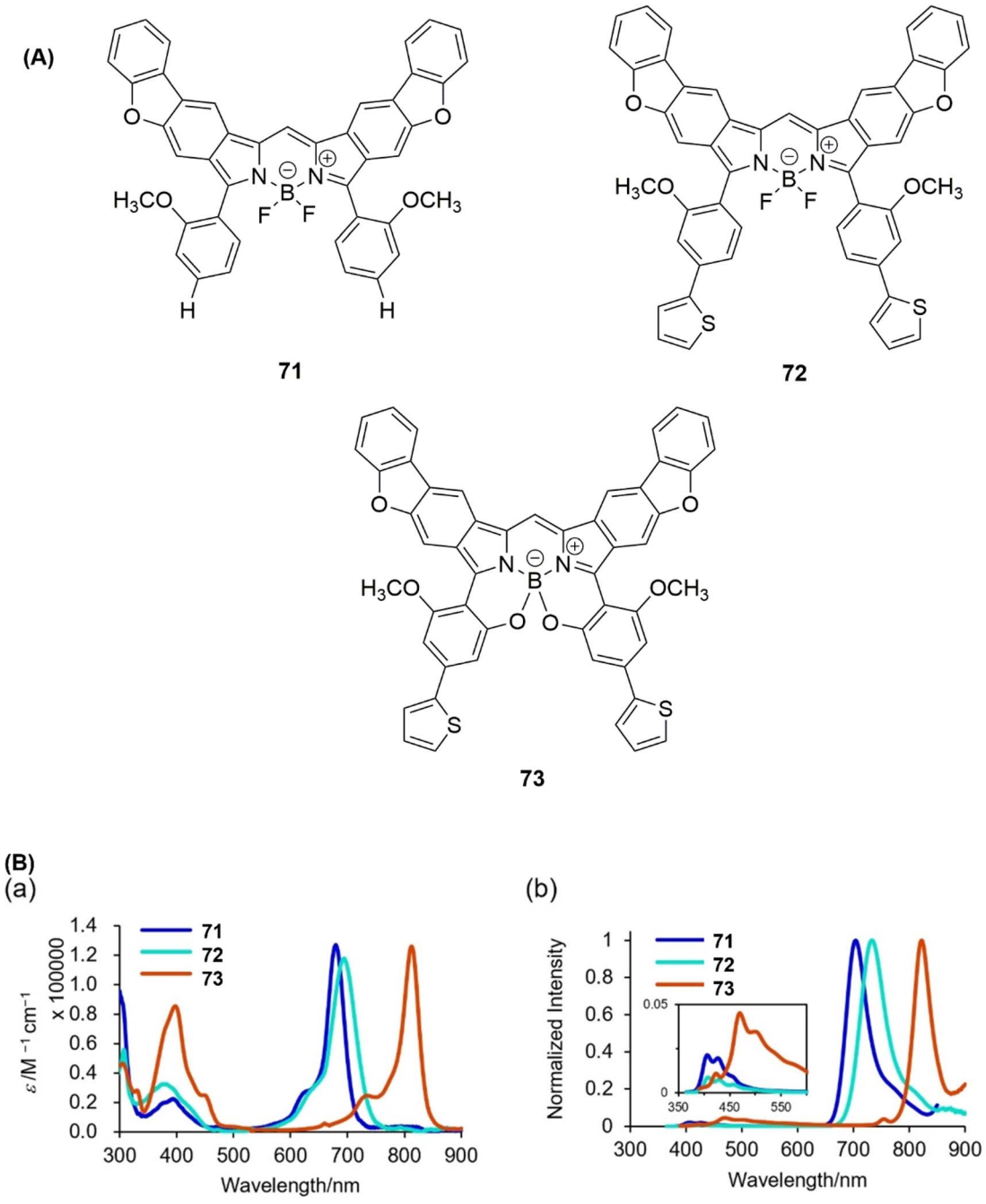

Fig. 25 (A) Chemical structure of dyes **71–73**. (B) (a) UV-vis absorption and (b) fluorescence emission spectra of compounds **71**, **72**, and **73** (1 μM) recorded in THF. Reproduced from ref. 104 with permission from Wiley, Copyright © 2025.

= 600 nm) (Fig. 28B(b)). In the solid state, as amorphous powders, **79c** maintained strong luminescence ($\Phi_F = 0.20$) with an even further blue-shifted emission at 531 nm. Conversely, the solid-state emission of **79a** and **79b** remained largely unchanged (λ_{em} = 672 and 518 nm, respectively), though their intensities were notably weak (Fig. 28B(c)).[107]

Hossan *et al.* (2025) reported the synthesis of four push–pull fluorescent thiophene–furan derivatives (**80–83**) (Fig. 29A). The optical properties of these compounds were systematically evaluated in solvents of varying polarity, revealing a pronounced influence of the medium on both absorption and fluorescence behavior. The nature of the aryl and thiophene–vinyl linkages, combined with the electron-donating substituents on the phenyl moiety (phenyl, anisyl, *n*-butyl, and dimethylamino groups), played a central role in tuning the absorption maxima. For instance, compound **80** showed the smallest Stokes shift in toluene (772 cm^{-1}), whereas the largest shift was observed in acetonitrile (1614 cm^{-1}), highlighting the

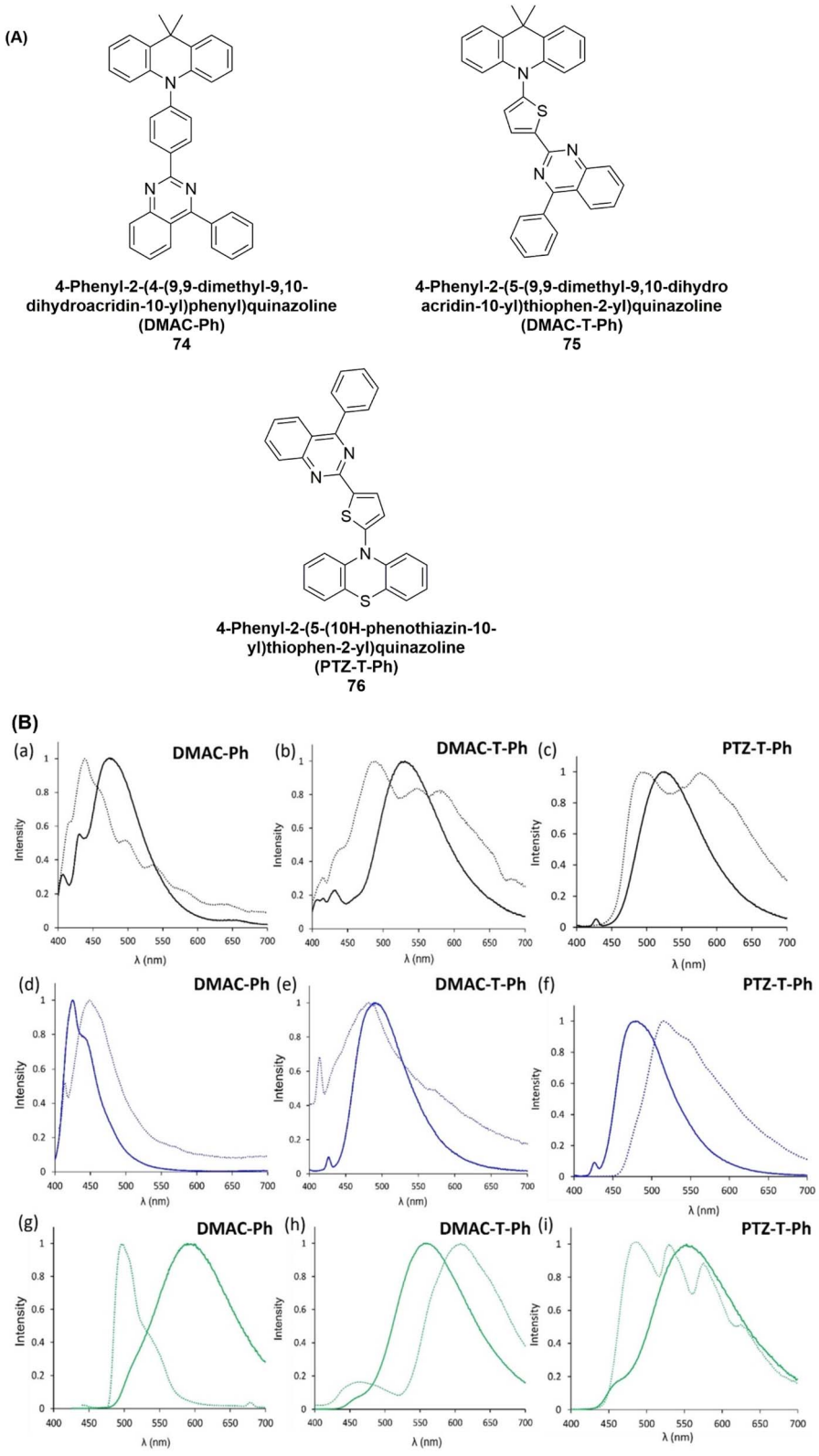

Fig. 26 (A) Chemical structure of DMAC-Ph (**74**), DMAC-T-Ph (**75**), and PTZ-T-Ph (**76**). (B) Normalized emission spectra of DMAC-Ph, DMAC-T-Ph, and PTZ-T-Ph recorded at 25 °C (solid lines) and 77 K (dotted lines) in (a–c) toluene, (d–f) *n*-heptane, and (g–i) Me-THF. Excitation wavelengths correspond to the respective absorption maxima. Reproduced from ref. 105 with permission from Wiley, Copyright © 2025, under the terms of the CC (BY-NC) 3.0 license.

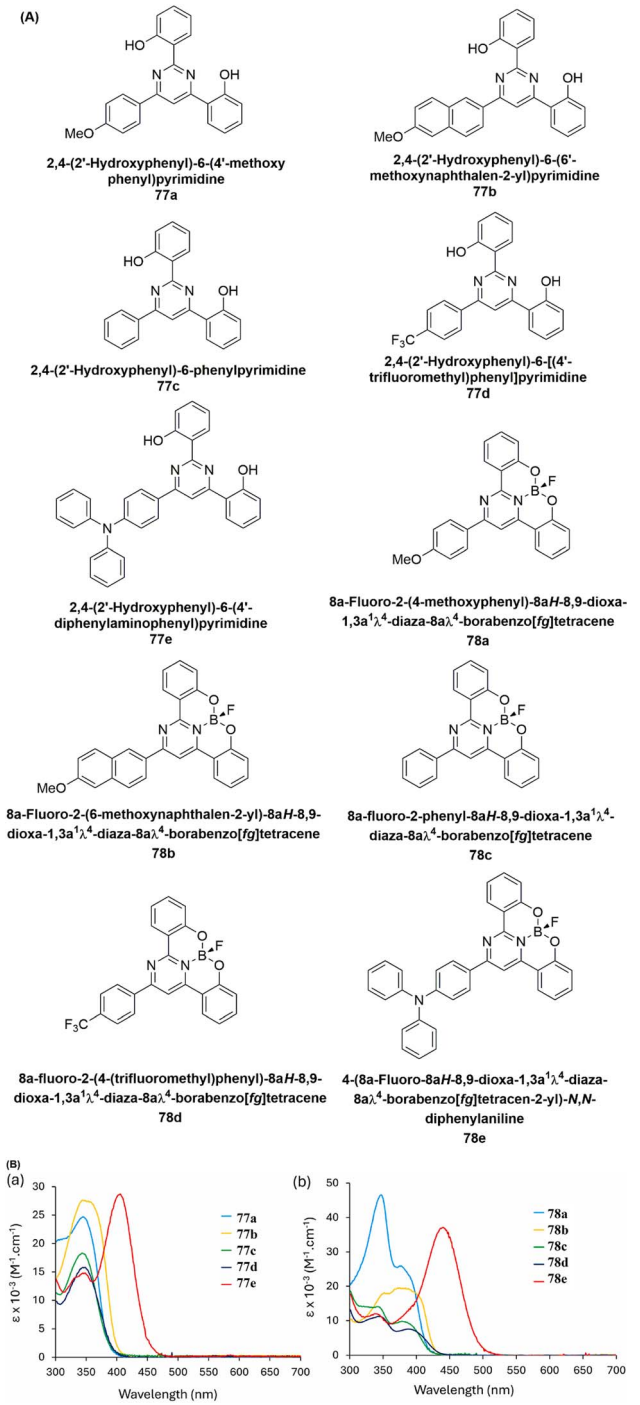

Fig. 27 (A) Chemical structure of compounds **77a–e** and **78a–e**. (B) UV-vis absorption spectra of (a) ligands **77a–e** and (b) their corresponding boron complexes **78a–e** recorded in CH_2Cl_2 solution. Reproduced from ref. 106 with permission from Elsevier, Copyright © 2025, under the terms of the CC (BY-NC) 3.0 license.

stabilization of the excited state in polar environments. Non-polar solvents, such as toluene, provided limited stabilization, resulting in larger energy gaps between absorption and emission, while polar solvents like ACN and DMSO enhanced solute–solvent interactions, leading to reduced gaps and altered emission profiles. Similarly, compound **81** displayed solvent-dependent shifts ranging from 732 cm^{-1} in toluene to 1270 cm^{-1} in DMSO. Particularly, **82** and **83** exhibited the most pronounced red-shifts in polar solvents, whereas minimal shifts were recorded in non-polar media (Fig. 29B). These findings underline the strong solvatochromic response of these derivatives, where both solvent polarity and hydrogen-bonding capacity significantly modulate fluorescence quantum yield and Stokes shift magnitude. Hydrogen bonding between the fluorophore and solvent molecules was particularly influential, altering excited-state stabilization and thereby modifying optical characteristics. In addition to their environment-sensitive emission, these compounds displayed high photostability, making them attractive candidates for long-term fluorescence imaging and sensing applications.[108]

Renuka *et al.* (2025) reported the photophysical properties of a newly synthesized fluorescein-based derivative, 2-(5-((2,4-dichlorophenyl)diazenyl)-6-hydroxy-3-oxo-3*H*-xanthen-9-yl) benzoic acid (2-DHOC **84**) (Fig. 30A). The absorption spectra of **84** recorded in solvents of varying polarity (Fig. 30B) display a broad absorption band with maxima ranging between 237–452 nm, along with a weaker band at the lower-energy side. These transitions are assigned to $\pi \rightarrow \pi^*$ excitations, which are modulated by ICT arising from the donor substituent linked to the fluorescein acceptor through a π-conjugated bridge. Although the ICT character in **84** is relatively weak, the spectra indicate localized $\pi \rightarrow \pi^*$ transitions with subtle ICT contributions. The absorption profiles remain nearly unchanged across solvents of different polarity; however, the band intensities are solvent-dependent. The highest absorption intensity is observed in DMSO ($\lambda_{max} = 324$ nm), while the lowest occurs in benzene at nearly the same wavelength. Minor spectral redshifts of 2–5 nm is detected on both the high- and low-energy sides, highlighting solvent polarity effects. The fluorescence spectra of 2-DHOC (**84**) were investigated at room temperature under excitation at 350 nm (Fig. 30B). In all solvents, a strong emission band appears at $\lambda_{max} \approx 517$ nm, with negligible change in band shape. Increasing solvent polarity induces a slight bathochromic shift in the emission maxima, with the largest shift (~5 nm) observed between DMSO and methanol. Only marginal shifts are noted in other solvents. These features render it a promising candidate for optical imaging applications and potential use in NLO devices, particularly those operating in the NIR region.[109]

Yin *et al.* (2025) synthesized and investigated bis-arylazo-naphthobipyrrole derivatives (**85–87**) bearing different substituents (–H, –Cl, and $–OCH_3$) (Fig. 31A). All three compounds display absorption maxima (λ_{max}) in the range of 534–549 nm and weak fluorescence between 599–628 nm, attributable to their extended π-conjugated frameworks. In addition, they exhibit solvatochromic responses, particularly in chlorinated solvents. Compound **85** shows a λ_{max} absorption band at 534 nm, which is red-shifted. This indicates enhanced π-conjugation arising from the interaction of two phenylazo groups with the naphthobipyrrole core. Compounds **86** and **87** exhibit further bathochromic shifts relative to **85**, likely due to the conjugative effect of the chlorine substituent in **86** and the

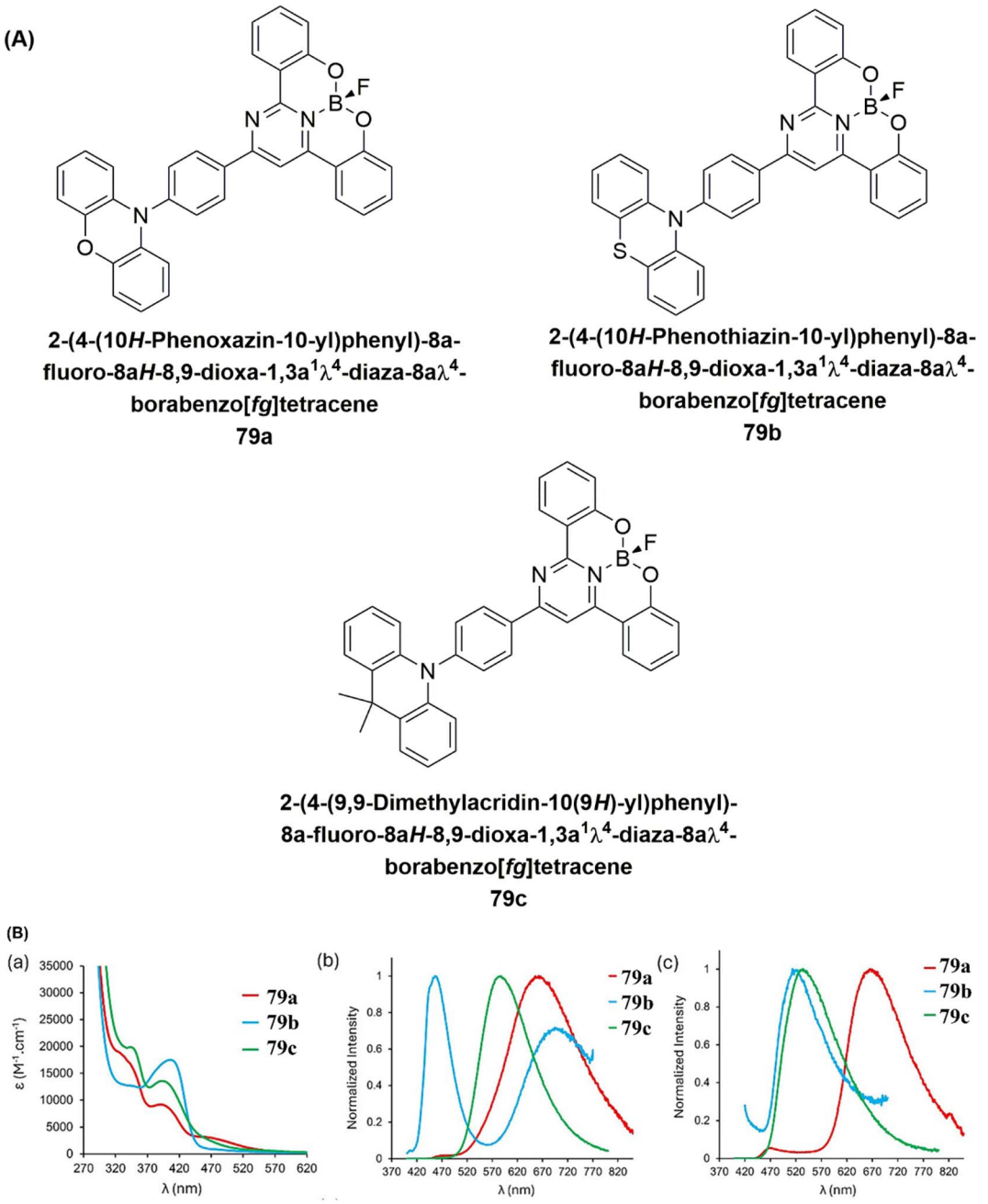

Fig. 28 (A) Chemical structure of pyrimidine-based boron complexes **79a–c**. (B) (a) Absorption spectra (b) normalized emission spectra ($c = 1$ μM) of boron complexes **79a–c** in toluene (c) normalized solid-state emission spectra of the same complexes recorded as amorphous powders. Reproduced from ref. 107 with permission from Wiley, Copyright © 2025, under the terms of the CC (BY-NC) 3.0 license.

strong electron-donating ability of the $-OCH_3$ group in **87**. Moreover, all three compounds (**85–87**) present shoulder bands between 507–516 nm, which are attributed to azo–hydrazone tautomerism. Among them, compound **87** shows the highest fluorescence intensity, consistent with the electron-donating influence of the methoxy substituent. Interestingly, in chlorinated solvents, the fluorescence bands of **85–87** shift further to 660, 677, and 720 nm, respectively, confirming their pronounced solvatochromic behavior (Fig. 31B).[110]

7 Structure–property relationship

Understanding the correlation between molecular structure and photophysical or electronic properties is critical for designing efficient push–pull heterocyclic systems. Structure–property relationship (SPR) analysis helps identify how various structural modifications influence parameters like absorption/emission wavelengths, quantum yields, charge mobility, and energy levels (Table 2).

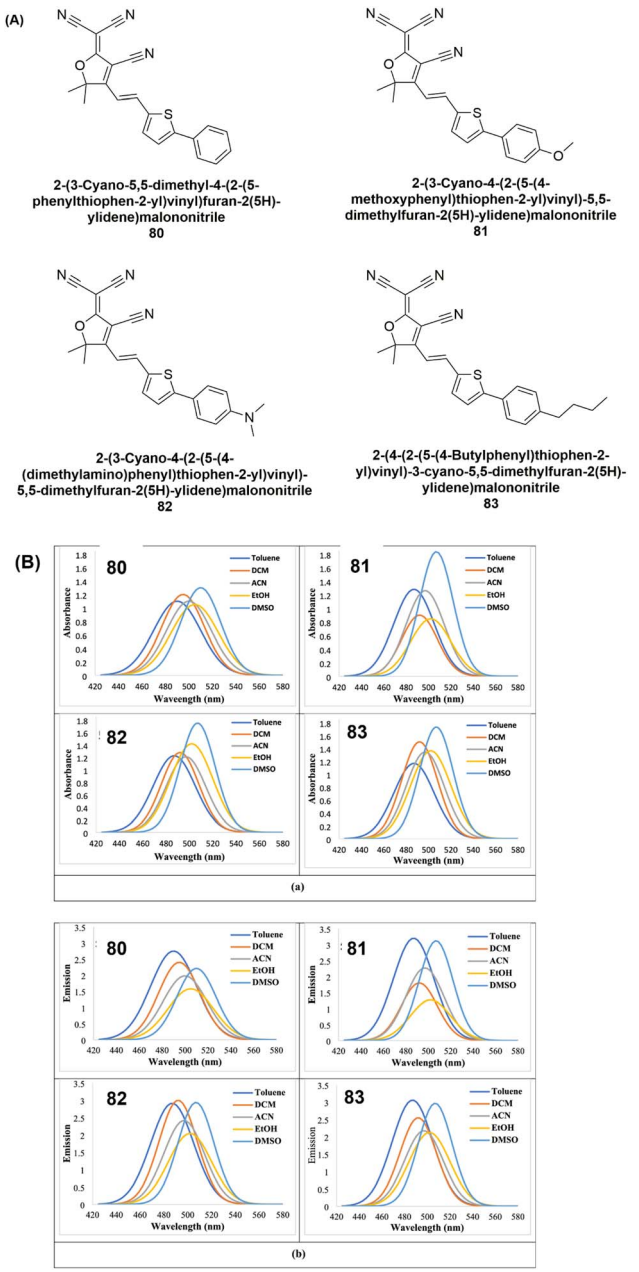

Fig. 29 (A) Chemical structure of fluorophores **80–83**. (B) (a) Absorption spectra and (b) fluorescence spectra of fluorophores **80–83**.[108]

The modulation of donor and acceptor units provides a direct and effective strategy for controlling the HOMO–LUMO energy levels, ICT strength, and spectral characteristics. Incorporation of electron-rich donors such as diphenylamine, carbazole, phenothiazine, or dimethylacridan typically raises the HOMO energy and induces a red shift in absorption and emission. Conversely, strong acceptors like nitro, cyano, dicyanovinyl, and benzothiadiazole lower the LUMO level, intensifying ICT and promoting NIR emission. For example, bisarylazo-naphthobipyrrole derivatives with –Cl and –OCH_3 substituents display bathochromic shifts compared to the unsubstituted analogue, attributed to enhanced donor–acceptor interactions and extended π-delocalization. Similarly, replacing a phenyl donor with a carbazole moiety in a D–π–A fluorophore results in a red shift of approximately 60–80 nm in the emission spectrum and improved quantum yield, demonstrating the critical role of donor strength in spectral tuning. For example, coumarin dyes bearing a (4-aminophenyl)ethynyl group at the 3-position exhibited nearly identical absorption maxima (~410 nm) but showed pronounced solvent-dependent emission behavior. Incorporation of stronger donor groups, such as dimethylamino, enhanced ICT, leading to more significant red-shifts and fluorescence quenching in polar solvents due to stabilization of the excited state and narrowing of the energy gap.

Beyond donor and acceptor modification, the type and length of the π-bridge significantly influence charge delocalization and transition energies. Incorporating thiophene, furan, phenylene–vinylene, or ethynylene bridges enhances electronic communication between donor and acceptor units, lowering the band gap and inducing red-shifted emission. In thiophene–furan-based ATVTCF analogues, variation in π-bridge and aryl substituents directly affects both absorption and Stokes shifts across different solvents, demonstrating how bridge engineering can modulate solvatochromic behavior. However, excessive conjugation may introduce non-radiative pathways or torsional disorder, leading to reduced PLQY. Benzothiazole conjugates with different donor and acceptor substituents displayed marked bathochromic shifts in both absorption and emission with increasing solvent polarity. Compounds with nitro and diphenylamino groups showed the highest absorption in DMSO, highlighting the role of strong electron-donating and withdrawing pairs in enhancing π–π* transitions. Stokes shift analyses further confirmed that stronger push–pull interactions lead to greater solvent reorganization energy and larger shifts.

Molecular geometry critically governs charge transport and radiative processes. Planar and rigid backbones promote efficient π–π stacking, which is advantageous for solid-state applications such as OLEDs and OFETs. In contrast, steric interactions between donor and acceptor units—especially in *ortho*-substituted systems—can lead to TICT states. These conformers, as observed in phenothiazine-based systems, give rise to dual emission bands attributed to quasi-equatorial and quasi-axial geometries. While TICT enhances solvatochromism, it may compromise emission intensity in condensed phases.

Strategic placement of substituents and solvent environment further refine the photophysical response of push–pull systems. Electron-donating groups such as alkoxy or amino substituents increase molecular polarity and dipole moments, thereby amplifying ICT transitions. Fluorination or introduction of electron-deficient groups can enhance molecular stability and tune emission wavelengths. Solvent polarity plays a pivotal role in stabilizing excited states, as evidenced by ATVTCF derivatives, which exhibit Stokes shifts ranging from ~700 cm^{-1} in non-polar solvents to >1600 cm^{-1} in polar media. These solvent-induced shifts highlight the sensitivity of push–pull systems to their surrounding environment, which can be exploited for

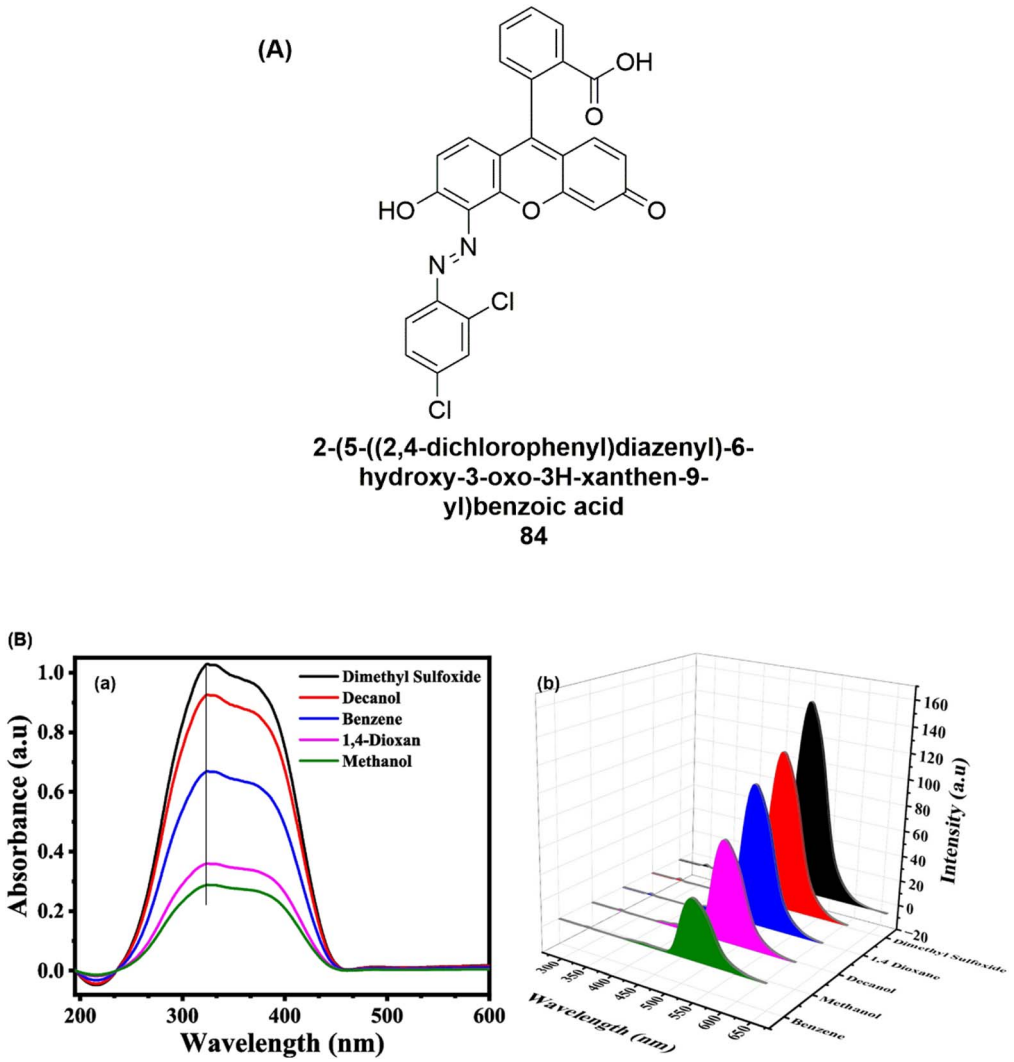

Fig. 30 (A) Chemical structure of 2-DHOC **84**. (B) (a) UV-vis absorption spectra (b) fluorescence spectra of the **84** in the same solvents.[109]

sensing, imaging, and tunable emission applications. Such tunability makes push–pull heterocycles highly versatile platforms for designing materials with tailored photophysical properties for sensing, imaging, and optoelectronic applications.

8 Comparative analysis and critical perspectives

The literature published during 2024–2025 demonstrates substantial progress in the design and application of push–pull heterocyclic systems, with a particular focus on donor–π–acceptor (D–π–A) architectures. Comparative evaluation reveals that the photophysical and electronic properties of these chromophores are primarily dictated by the strength of donor and acceptor groups, the nature of the π-conjugated bridge, and molecular conformation.

Donor strength plays a decisive role in tuning the electronic structure. Strong electron donors such as carbazole, phenothiazine, and diphenylamine consistently elevate the HOMO energy level, facilitating ICT and inducing bathochromic shifts in absorption and emission spectra. When coupled with potent electron-withdrawing groups like dicyanovinyl, benzothiadiazole, or nitro substituents, these systems exhibit enhanced ICT efficiency, narrow bandgaps, and NIR emission, making them attractive for optoelectronic and sensing applications. For example, carbazole-based D–π–A fluorophores have been reported to exhibit red shifts of 60–80 nm alongside improved quantum yields.

The incorporation of extended π-bridges, such as thiophene, phenylene–vinylene, or ethynylene units, improves delocalization and reduces the optical bandgap, further red-shifting the emission. However, excessive extension of π-conjugation can promote conformational twisting, thereby enhancing non-radiative decay pathways and diminishing photoluminescence quantum yield (PLQY). Thus, optimizing bridge length is essential for achieving both strong ICT and high luminescence efficiency.

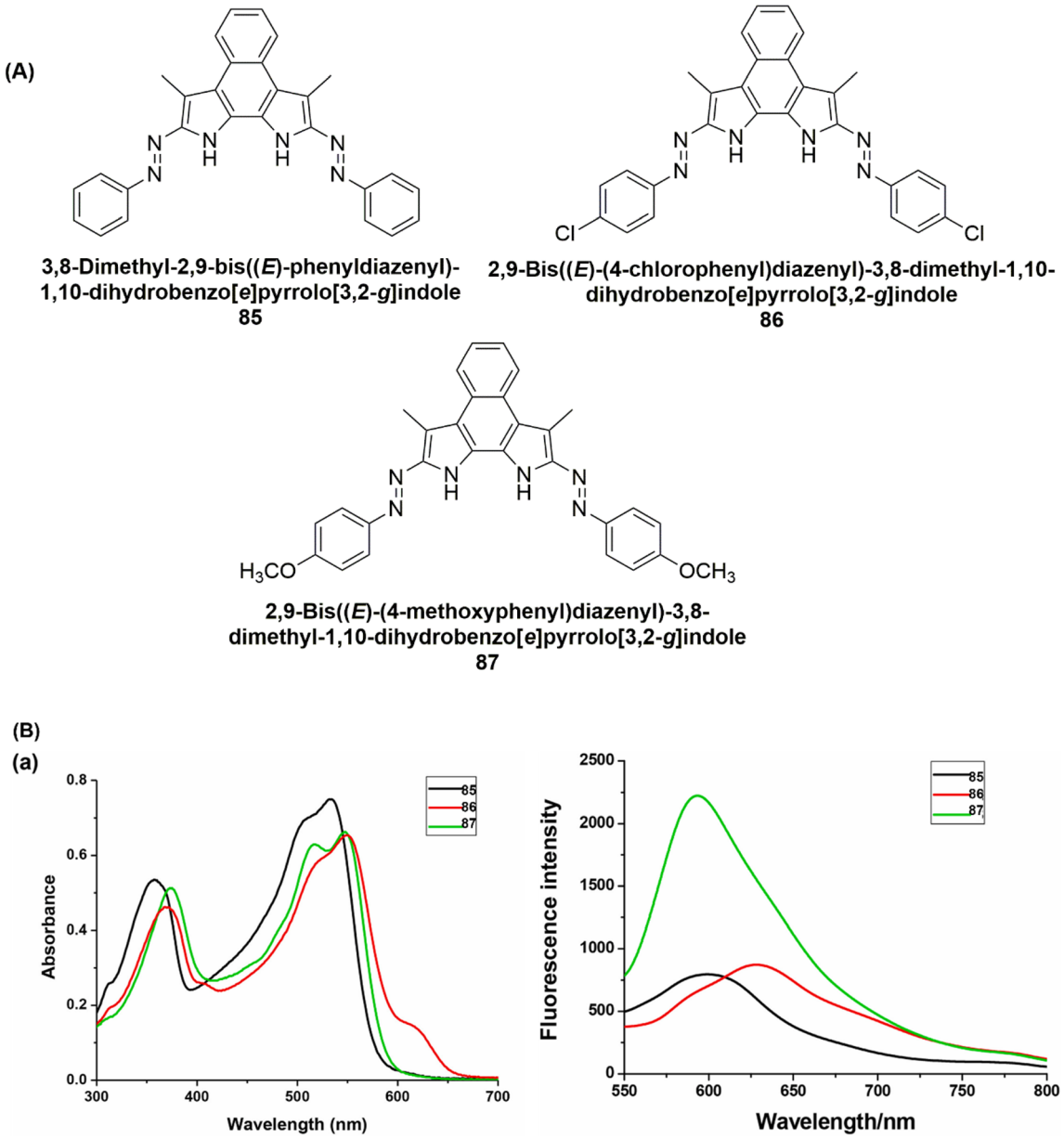

Fig. 31 (A) Chemical structure of naphthobipyrroles **85–87**. (B) (a) UV-vis absorption spectra (b) fluorescence emission spectra of compounds **85–87** in CH_3CN solution (2×10^{-5} M). Reproduced from ref. 110 with permission from Elsevier, Copyright © 2025.

Molecular planarity emerges as another critical determinant of performance. Planar structures favor π–π stacking and high charge mobility, which are desirable for solid-state devices such as OLEDs and OFETs. Conversely, sterically hindered or twisted conformations often give rise to TICT states, which enhance solvatochromism but compromise solid-state emission. Structural modifications incorporating bulky substituents can mitigate ACQ, often giving rise to aggregation-induced emission enhancement (AIEE), thereby improving performance in condensed phases.

Table 2 Structure–photophysical property trends

Structural change	Photophysical outcome
Stronger donor/acceptor	Red-shifted λ_{max}, enhanced ICT
Longer π-bridge	Lower bandgap, but risk of PL quenching
Planar structure	Enhanced charge transport, higher PLQY
Twisted conformation	Solvatochromism, possible AIE behavior
Bulky side groups	Solid-state emission enhancement (AIEE)

Despite these advances, several challenges remain. Many high-performance D–π–A systems suffer from ACQ effects, limiting their practical application in solid-state devices. While AIE-active designs offer a potential solution, balancing luminescence efficiency with charge transport remains unresolved. Additionally, although computational approaches such as DFT and TD-DFT have provided mechanistic insights into ICT and photophysical behavior, experimental validation under real

Table 3 Comparative evaluation of structural modifications and their photophysical consequences in push–pull heterocyclic systems

Structural parameter	Positive effects	Limitations/critics	Best reported examples (2024–2025)
Strong donor (carbazole, phenothiazine, diphenylamine)	Elevated HOMO, bathochromic shifts, high PLQY, enhanced ICT	Reduced stability under oxidative conditions	Carbazole-based fluorophores (60–80 nm red shift)
Potent acceptor (dicyanovinyl, benzothiadiazole, nitro, cyano)	Lowered LUMO, strong ICT, efficient NIR emission	Excessive non-radiative decay may reduce quantum yield	Benzothiadiazole-based OLED scaffolds
Extended π-bridge (thiophene, phenylene–vinylene, ethynylene)	Improved conjugation, reduced bandgap, red-shifted emission	Excessive length $\rightarrow$ twisting, ACQ, reduced PLQY	Thiophene–phenylene–vinylene hybrids
Planarity	Enhanced charge mobility, strong π–π stacking, higher device performance	May induce aggregation and self-quenching	Linear carbazole–benzothiadiazole systems
Twisted/TICT conformation	Solvatochromism, tunable emission	Weak solid-state luminescence	*Ortho*-substituted donor–acceptor dyes
Bulky substituents (AIEE design)	Suppresses ACQ, enhances solid-state luminescence	Reduced charge transport if excessive	Tetraphenylethene-modified D–π–A systems
Substituent effects (alkoxy, amino, fluorine)	Tailored dipole moments, polarity, and stability	Misplaced substituents may disrupt conjugation	Fluorinated carbazole-based chromophores

device-operating conditions remains scarce. A comparative summary of the structure–property trends is presented in Table 3.

Hence, carbazole- and phenothiazine-derived donors in combination with strong acceptors such as benzothiadiazole or dicyanovinyl, bridged by optimally extended π-systems, represent the most efficient push–pull heterocyclic frameworks reported during 2024–2025. While significant progress has been achieved, overcoming ACQ effects, improving device-level stability, and integrating theoretical predictions with experimental validations remain key challenges for the development of next-generation functional materials.

9 Challenges and future perspectives

Despite significant progress in the development of push–pull heterocyclic systems, several critical challenges remain that hinder their widespread application in optoelectronic devices and photonic technologies.

9.1 Thermal and photostability

One of the key limitations of D–π–A systems is their poor long-term thermal or photostability, especially under continuous irradiation. Electron-rich donors and extended π-systems are prone to oxidation, while acceptors such as cyano groups can undergo degradation. Developing systems with rigid backbones, incorporating sterically protected donors/acceptors, or using cyclic acceptor motifs (*e.g.*, triazines) can improve durability.

9.2 Aggregation-induced quenching (ACQ)

Planar push–pull systems often exhibit ACQ due to π–π stacking in the solid state, which leads to non-radiative decay pathways and limits device performance. Designing AIE-active systems, using twisted backbones, or introducing bulky side chains to prevent stacking offers a route to mitigate ACQ.

9.3 Solubility and processability

Highly conjugated or rigid molecules usually suffer from poor solubility, which affects solution-processing techniques such as spin-coating and inkjet printing. Molecular engineering to incorporate solubilizing groups (*e.g.*, alkyl chains, oligoethylene glycols) can address this limitation.

9.4 Control of excited-state dynamics

Managing intersystem crossing, exciton diffusion, or triplet harvesting is crucial in applications like OLEDs and photocatalysis. However, the fine-tuning of ΔE_{ST} or lifetime remains nontrivial. Computational design using TD-DFT or machine learning to pre-screen TADF or RTP-active candidates is a promising strategy.

9.5 Sustainability and green chemistry

Many synthetic routes for push–pull systems rely on toxic solvents, metal catalysts, or multi-step purifications, which

raise environmental and economic concerns. Adopting green oxidants, solvent-free methods, or click chemistry can reduce environmental impact and increase scalability.

9.6 Device integration and performance

Although many push–pull systems demonstrate excellent solution-phase behavior, translating these properties into solid-state devices such as OLEDs, OFETs, or DSSCs requires interface compatibility, charge injection balance, and layer uniformity. Integration with hybrid materials, polymer matrices, or self-assembled monolayers (SAMs) may facilitate better device fabrication.

Henceforth, future research should aim to synergize theoretical modeling, synthetic chemistry, and device engineering to overcome these limitations and unlock the full potential of push–pull heterocyclic materials in next-generation optoelectronics.

10 Conclusions

Recent advances in the design and development of heterocyclic push–pull chromophores have provided significant insights into their photophysical behaviors, synthetic strategies, and functional applications. Studies published in 2024–2025 highlight how structural modifications—such as the introduction of electron-donating and electron-withdrawing groups, heteroaryl substituents, and extended π-conjugation—directly influence absorption–emission profiles, ICT, AIE, and bandgap tuning. Environmentally friendly methodologies, including deep eutectic solvents, microwave-assisted protocols, and efficient cycloaddition reactions, have further expanded the sustainable synthesis of these advanced materials. The investigations discussed in this review reveal the critical role of donor–acceptor interactions and structural engineering in tailoring photophysical efficiency, fluorescence intensity, and spectral shifts. Compounds such as indolyl–coumarin hybrids, 3-cyano-2-pyridones, TCBD derivatives, and modified BODIPYs exemplify the potential of heterocyclic scaffolds in achieving desirable optical properties, spanning from UV-visible to the NIR. These findings not only deepen our understanding of molecular structure–property relationships but also underscore the potential of these systems in applications such as optoelectronics, sensing, imaging, and photodetection. For the first time, we have comprehensively summarized and analyzed the literature from 2024 to 2025, providing a timely overview of the current state of research. This consolidation of knowledge will assist researchers in identifying new directions for molecular design and in advancing the development of high-performance, multifunctional heterocyclic materials.

Author contributions

Manel Essid: data curation, funding acquisition. Ehsan Ullah Mughal: main idea, data analysis and collection, reviewing and editing, final writing the manuscript.

Conflicts of interest

The author has no conflicts of interest to declare.

Data availability

No primary research results, software or code have been included and no new data were generated or analyzed as part of this review (only for review articles).

Acknowledgements

The authors extend their appreciation to the Deanship of Research and Graduate Studies at King Khalid University for funding this work through Large Research Project under grant number RGP2/148/46.

References

1 A. Mishra and P. Bäuerle, *Angew. Chem., Int. Ed.*, 2012, **51**, 2020–2067.
2 F. Würthner, *Acc. Chem. Res.*, 2016, **49**, 868–876.
3 Y. Li, *Acc. Chem. Res.*, 2012, **45**, 723–733.
4 C. Coluccini, A. K. Sharma, M. Caricato, A. Sironi, E. Cariati, S. Righetto, E. Tordin, C. Botta, A. Forni and D. Pasini, *Phys. Chem. Chem. Phys.*, 2013, **15**, 1666–1674.
5 W. Su, Y. Weng, L. Jiang, Y. Yang, L. Zhao, Z. Chen, Z. Li and J. Li, *Org. Prep. Proced. Int.*, 2010, **42**, 503–555.
6 X. Xie, B. Lu, W. Li and Z. Zhang, *Coord. Chem. Rev.*, 2018, **355**, 39–53.
7 P. Kaur and K. Singh, *Chem. Rec.*, 2022, **22**, e202200024.
8 S. Kolemen and E. U. Akkaya, *Coord. Chem. Rev.*, 2018, **354**, 121–134.
9 L. Zhang, C. Li and S. Pang, *Coord. Chem. Rev.*, 2026, **546**, 217081.
10 W. Vallejo, M. Lerma and C. Díaz-Uribe, *Heliyon*, 2025, **11**, 1–19.
11 B. K. Korir, J. K. Kibet and S. M. Ngari, *Energy Sci. Eng.*, 2024, **12**, 3188–3226.
12 X. Ma, L. Shi, B. Zhang, L. Liu, Y. Fu and X. Zhang, *Anal. Bioanal. Chem.*, 2022, **414**, 4551–4573.
13 D. Si, Q. Li, Y. Bao, J. Zhang and L. Wang, *Angew. Chem., Int. Ed.*, 2023, **62**, e202307641.
14 B. Jordan, M. Pollier, Y. Ofir, S. Joubanian and J. Mehtala, *Chem. Commun.*, 2008, **1653**, 1653.
15 B. Patrizi, C. Cozza, A. Pietropaolo, P. Foggi and M. Siciliani de Cumis, *Molecules*, 2020, **25**, 430.
16 Q. Ye, L. Li, J. Zhang, M. Teng, F. Wu and D. Han, *Appl. Organomet. Chem.*, 2025, **39**, e70374.
17 F. Ding, Y. Zhan, X. Lu and Y. Sun, *Chem. Sci.*, 2018, **9**, 4370–4380.
18 M. Ma, S. Wang, S. Yu, X. Zeng and Z. Liu, *J. Mol. Struct.*, 2025, 143214.
19 R. Wang, J. Yuan, R. Wang, G. Han, T. Huang, W. Huang, J. Xue, H. C. Wang, C. Zhang and C. Zhu, *Adv. Mater.*, 2019, **31**, 1904215.

20 H. Zhu, X. Wang, R. Ma, Z. Kuang, Q. Guo and A. Xia, *ChemPhysChem*, 2016, **17**, 3245–3251.
21 M. Liu, X. Yu, M. Li, N. Liao, A. Bi, Y. Jiang, S. Liu, Z. Gong and W. Zeng, *RSC Adv.*, 2018, **8**, 12573–12587.
22 R. Lalitha and S. Velmathi, *J. Fluoresc.*, 2024, **34**, 15–118.
23 M. K. Goshisht, N. Tripathi, G. K. Patra and M. Chaskar, *Chem. Sci.*, 2023, **14**, 5842–5871.
24 X.-C. Chi, M.-C. Ni, Y.-H. Wang, N. Sui, W.-Y. Wang, R. Lu, Y.-Q. Yang, W.-Y. Ji and H.-Z. Zhang, *J. Photochem. Photobiol., A*, 2017, **346**, 221–224.
25 T. Stoerkler, G. Ulrich, P. Retailleau, A. D. Laurent, D. Jacquemin and J. Massue, *Chem. Sci.*, 2024, **15**, 7206–7218.
26 F. Würthner, T. E. Kaiser and C. R. Saha-Möller, *Angew. Chem., Int. Ed.*, 2011, **50**, 3376–3410.
27 C. J. Lu, Q. Xu, J. Feng and R. R. Liu, *Angew. Chem., Int. Ed.*, 2023, **62**, e202216863.
28 P. Kaur, M. Kaur, G. Depotter, S. Van Cleuvenbergen, I. Asselberghs, K. Clays and K. Singh, *J. Mater. Chem.*, 2012, **22**, 10597–10608.
29 P. Murugan, T. Hu, X. Hu and Y. Chen, *J. Mater. Chem. A*, 2022, **10**, 5044–5081.
30 R. García, J. Calbo, R. Viruela, M. Á. Herranz, E. Ortí and N. Martín, *ChemPlusChem*, 2018, **83**, 300–307.
31 J. Mei, Y. Hong, J. W. Lam, A. Qin, Y. Tang and B. Z. Tang, *Adv. Mater.*, 2014, **26**, 5429–5479.
32 Z. Qi, Z. An, B. Huang, M. Wu, Q. Wu and D. Jiang, *Org. Biomol. Chem.*, 2023, **21**, 6419–6423.
33 J. Mei, N. L. Leung, R. T. Kwok, J. W. Lam and B. Z. Tang, *Chem. Rev.*, 2015, **115**, 11718–11940.
34 A. Mishra, M. K. Fischer and P. Bäuerle, *Angew. Chem., Int. Ed.*, 2009, **48**, 2474–2499.
35 Q. Meng, S. Tan, X. Wen and J. Qiao, *Organic Electroluminescence: from Molecular Structure to Device Performance*, 2025, pp. 147–188.
36 K. Keerthika, V. Nutalaptai and R. kumar Konidena, *J. Mater. Chem. C*, 2025, 1–9.
37 S. Ghara, P. Barik, S. Ghosh, S. Ghosh, A. Mandal, C. Pramanik, M. Ikbal, S. Dhara and S. Samanta, *Org. Chem. Front.*, 2025, **12**, 2790–2837.
38 S. R. Forrest, *Organic Electronics: Foundations to Applications*, Oxford University Press, USA, 2020.
39 P. Leriche, P. Frère, P. Blanchard, A. Cravino and J. Roncali, *Tetrahedron Lett.*, 2009, **50**(40), 5673–5676.
40 S. Flammini, M. Di Sante, P. E. Costantini, E. J. Mattioli, A. Marconi, E. Turrini, S. La Rosa, M. Montrone, T. D. Marforio and M. Nigro, *J. Mater. Chem. B*, 2025, 1–10.
41 C. Rothe, D. Neusser, N. Hoppe, K. Dirnberger, W. Vogel, S. Gámez-Valenzuela, J. T. L. Navarrete, B. Villacampa, M. Berroth and M. C. R. Delgado, *Phys. Chem. Chem. Phys.*, 2020, **22**, 2283–2294.
42 Y. Li, J. Hu, G. He, H. Zhu, X. Wang, Q. Guo, A. Xia, Y. Lin, J. Wang and X. Zhan, *J. Phys. Chem. C*, 2016, **120**, 13922–13930.
43 A. Afrin, *Mater. Chem. Front.*, 2025, 1794–1820.
44 A. M. Asiri, O. I. Osman, S. H. Al-Thaqafy and S. A. Khan, *RSC Adv.*, 2017, **7**, 8402–8414.
45 R. D. Telore and N. Sekar, *J. Fluoresc.*, 2016, **26**, 1261–1270.
46 H. Mudila, P. Prasher, M. Kumar, A. Kumar, M. Zaidi and A. Kumar, *Mater. Renew. Sustain. Energy*, 2019, **8**, 9.
47 E. Keleş, M. Yahya, E. Aktan, B. Aydıner, N. Seferoğlu, A. Barsella and Z. Seferoğlu, *J. Photochem. Photobiol., A*, 2020, **402**, 112818.
48 K. Schwärzer, S. K. Rout, D. Bessinger, F. Lima, C. E. Brocklehurst, K. Karaghiosoff, T. Bein and P. Knochel, *Chem. Sci.*, 2021, **12**, 12993–13000.
49 M. Hancharova, K. Mazur, K. Halicka and D. Zając, *J. Polym. Res.*, 2022, **29**, 417.
50 E. V. Nosova, G. N. Lipunova, G. V. Zyryanov, V. N. Charushin and O. N. Chupakhin, *Org. Chem. Front.*, 2022, **9**, 6646–6683.
51 V. Dávila Cerón, L. A. Illicachi and B. Insuasty, *Molecules*, 2022, **28**, 257.
52 S. Qu and H. Tian, *Chem. Commun.*, 2012, **48**, 3039–3051.
53 R. K. Kanaparthi, J. Kandhadi and L. Giribabu, *Tetrahedron*, 2012, **68**, 8383–8393.
54 J. Balam-Villarreal, B. López-Mayorga, D. Gallardo-Rosas, R. Toscano, M. Carreón-Castro, V. Basiuk, F. Cortés-Guzmán, J. López-Cortés and M. Ortega-Alfaro, *Org. Biomol. Chem.*, 2020, **18**, 1657–1670.
55 E. González-Rodríguez, B. Guzman-Juarez, M. Miranda-Olvera, M. del Pilar Carreón-Castro, M. Maldonado-Domínguez, R. Arcos-Ramos, N. Farfan and R. Santillan, *Spectrochim. Acta, Part A*, 2022, **267**, 120520.
56 G. Noirbent, D. Brunel, T.-T. Bui, S. Péralta, P.-H. Aubert, D. Gigmes and F. Dumur, *New J. Chem.*, 2021, **45**, 13475–13498.
57 J. Rouillon, C. Benitez-Martin, M. Grøtli and J. Andréasson, *Phys. Chem. Chem. Phys.*, 2025, **27**, 4679–4685.
58 D. Beljonne, T. Kogej, S. Marder, J. Perry and J. Bredas, *Mol. Cryst. Liq. Cryst. Sci. Technol., Sect. BNonlinear Opt.*, 1999, **21**, 461–480.
59 F. Terenziani, C. Katan, E. Badaeva, S. Tretiak and M. Blanchard-Desce, *Adv. Mater.*, 2008, **20**, 4641–4678.
60 C. Xu and W. W. Webb, *J. Opt. Soc. Am. B*, 1996, **13**, 481–491.
61 R. Cui, Y. Zou, L. Xiao, C.-S. Hsu, M. L. Keshtov, D. Y. Godovsky and Y. Li, *Dyes Pigm.*, 2015, **116**, 139–145.
62 M. Albota, D. Beljonne, J.-L. Bredas, J. E. Ehrlich, J.-Y. Fu, A. A. Heikal, S. E. Hess, T. Kogej, M. D. Levin and S. R. Marder, *Science*, 1998, **281**, 1653–1656.
63 G. S. He, L.-S. Tan, Q. Zheng and P. N. Prasad, *Chem. Rev.*, 2008, **108**, 1245–1330.
64 B. A. Reinhardt, L. L. Brott, S. J. Clarson, A. G. Dillard, J. C. Bhatt, R. Kannan, L. Yuan, G. S. He and P. N. Prasad, *Chem. Mater.*, 1998, **10**, 1863–1874.
65 F. Terenziani, M. Morone, S. Gmouh and M. Blanchard-Desce, *ChemPhysChem*, 2006, **7**, 685–696.
66 C. F. Calver, K. S. Schanze and G. Cosa, *ACS Nano*, 2016, **10**, 10598–10605.
67 M. Pawlicki, H. A. Collins, R. G. Denning and H. L. Anderson, *Angew. Chem., Int. Ed.*, 2009, **48**, 3244–3266.
68 N. S. Makarov, M. Drobizhev and A. Rebane, *Opt. Express*, 2008, **16**, 4029–4047.

69 B. Carlotti, E. Benassi, V. Barone, G. Consiglio, F. Elisei, A. Mazzoli and A. Spalletti, *ChemPhysChem*, 2015, **16**, 1440–1450.
70 X. Feng, X. Wang, C. Redshaw and B. Z. Tang, *Chem. Soc. Rev.*, 2023, **52**, 6715–6753.
71 Z. Zhao, H. Zhang, J. W. Lam and B. Z. Tang, *Angew. Chem., Int. Ed.*, 2020, **59**, 9888–9907.
72 C. Botta, S. Benedini, L. Carlucci, A. Forni, D. Marinotto, A. Nitti, D. Pasini, S. Righetto and E. Cariati, *J. Mater. Chem. C*, 2016, **4**, 2979–2989.
73 Q. Yan and S. Wang, *Mater. Chem. Front.*, 2020, **4**, 3153–3175.
74 A. Nitti and D. Pasini, *Handbook of Aggregation-Induced Emission*, 2022, pp. 575–608.
75 R. J. Durand, S. Gauthier, S. Achelle, T. Groizard, S. Kahlal, J.-Y. Saillard, A. Barsella, N. Le Poul and F. R. Le Guen, *Dalton Trans.*, 2018, **47**, 3965–3975.
76 D. Mirani, A. J. Riquelme, S. Fauvel, C. Aumaître, P. Maldivi, J. Pécaut and R. Demadrille, *Mater. Chem. Front.*, 2025, 2770–2783.
77 O. P. Dimitriev, *Chem. Rev.*, 2022, **122**, 8487–8593.
78 M. Fang, J. Yang and Z. Li, *Prog. Mater. Sci.*, 2022, **125**, 100914.
79 Y. Meng, W. Liu, Z. Liu, M. Gao, M. Fang, J. Yang, D. Ma and Z. Li, *ACS Appl. Mater. Interfaces*, 2024, **16**, 60658–60665.
80 S. Hirata, Y. Sakai, K. Masui, H. Tanaka, S. Y. Lee, H. Nomura, N. Nakamura, M. Yasumatsu, H. Nakanotani and Q. Zhang, *Nat. Mater.*, 2015, **14**, 330–336.
81 S. Zaman, M. Wang, H. Liu, F. Sun, Y. Yu, J. Shui, M. Chen and H. Wang, *Trends Chem.*, 2022, **4**, 886–906.
82 D. Pant, *Effects of Various Bridges on Linear and Nonlinear Optical Properties of Some Push-Pull Type of Organic Molecules*, University of Johannesburg, South Africa, 2021.
83 G. Feng, Z. Li, P. Zhai, M. Ying, Z. Xu, C. Yang, X. Wang, B. Dong, K.-T. Yong and G. Xu, *Sens. Actuators, B*, 2022, **371**, 132577.
84 X. Liang, J. Liu, C. Dong, Y. Li, C. Zhao and C. Li, *Dyes Pigm.*, 2025, 112940.
85 R. N. Bennett, A. D. Hendsbee, J. H. Ngai, A. Ganguly, Y. Li and T. L. Kelly, *ACS Appl. Electron. Mater.*, 2020, **2**, 2039–2048.
86 A. Wadsworth, M. Moser, A. Marks, M. S. Little, N. Gasparini, C. J. Brabec, D. Baran and I. McCulloch, *Chem. Soc. Rev.*, 2019, **48**, 1596–1625.
87 J. Sarrato, B. Raimundo, L. Domingues, S. R. Filipe, J. C. Lima and P. S. Branco, *Dyes Pigm.*, 2024, **228**, 112204.
88 I. Zghab and A. N. Alanazi, *J. Photochem. Photobiol., A*, 2024, **454**, 115688.
89 A. E. Kopotilova, M. I. Valieva, E. A. Kudryashova, E. S. Starnovskaya, T. N. Moshkina, E. V. Nosova, O. S. Taniya, A. A. Kalinichev, A. S. Novikov and D. S. Kopchuk, *Asian J. Org. Chem.*, 2024, **13**, e202400135.
90 T. N. Moshkina, A. E. Kopotilova, M. A. Ivan'kina, E. S. Starnovskaya, D. A. Gazizov, E. V. Nosova, D. S. Kopchuk, O. S. El'tsov, P. A. Slepukhin and V. N. Charushin, *Molecules*, 2024, **29**, 2497.
91 P. Krawczyk, B. Jędrzejewska, J. Cytarska, K. Seklecka and K. Z. Łączkowski, *Sensors*, 2024, **24**, 6368.
92 K. S. Salih and A. M. Shraim, *Push-Pull Functional Asymmetric Azines: Understanding the Intramolecular Charge Transfer Fluorescence, and Solvatochromism*, 2024.
93 W. Kim, R. Manivannan and Y.-A. Son, *J. Fluoresc.*, 2024, 1–19.
94 J. M. Gonçalves, J. N. Gonçalves, L. F. Sousa, L. R. Rodrigues, P. Correia-de-Sá, P. J. Coutinho, E. M. Castanheira, R. Oliveira and A. M. Dias, *Org. Biomol. Chem.*, 2024, **22**, 2252–2263.
95 A. D. Bani-Yaseen, M. Shkoor, V. Thotathil, E. G. Mohammad, H. Mehanna and R. M. Al-Zoubi, *J. Lumin.*, 2025, **280**, 121064.
96 A. P. Potapova, O. S. Taniya, M. I. Valieva, I. A. Khalymbadzha, A. D. Sharapov, E. S. Starnovskaya, D. S. Kopchuk, V. S. Gaviko, A. S. Novikov and A. A. Kalinichev, *Opt. Mater.*, 2025, **158**, 116471.
97 B. Karagöllü, T. O. Şengöz, H. Kayaş, K. Erden, E. Şahin, O. Esenturk and C. Dengiz, *Dyes Pigm.*, 2025, **232**, 112469.
98 Y. Zhang, S. Liu, R. Zhao, Y. Xu, H. Zhao, Z. Song, Y. Mao, J. Tang and X. Wang, *J. Lumin.*, 2025, **278**, 121001.
99 G. Y. Erdemir, *J. Fluoresc.*, 2025, 1–8.
100 S. Suresha, G. Shilpa, Q. Mohsen, A. M. Alsuhaibani, C. Pandurangappa, P. Prabhala and M. Thippeswamy, *J. Fluoresc.*, 2025, 1–14.
101 T. L. Devi, M. M. Devi and O. M. Singh, *ChemistrySelect*, 2025, **10**, e03785.
102 S. Sangwan, R. Kumar, J. Sindhu, S. Chauhan, N. Yadav, V. Dhanda and A. Duhan, *ChemistrySelect*, 2025, **10**, e01271.
103 X. Chen and T. Michinobu, *J. Org. Chem.*, 2025, **90**, 1561–1570.
104 A. Suzuki, R. Yamamoto, M. Ito and Y. Kubo, *ChemPlusChem*, 2025, **90**, e202500021.
105 M. Hodée, T. N. Moshkina, J. Massue, A. Fihey, T. Roisnel, C. Katan, E. Nosova and S. Achelle, *ChemPhotoChem*, 2025, **9**, e202400259.
106 C. Diguet, A. Navarro, M. P. Fernández-Liencres, S. B. Jiménez-Pulido, N. A. Illán-Cabeza, J. Massue, S. Gauthier, F. Robin-le Guen, S. Achelle and J. Rodríguez-López, *Dyes Pigm.*, 2025, **236**, 112660.
107 C. Diguet, A. Navarro, M. P. Fernández-Liencres, S. B. Jiménez-Pulido, N. A. Illán-Cabeza, A. Almutairi, D. Tondelier, S. Gauthier, F. Robin-le Guen and J. Rodríguez-López, *Chem.–Eur. J.*, 2025, **31**, e202501089.
108 A. Hossan, *Arabian J. Sci. Eng.*, 2025, 1–12.
109 M. Sucheta, A. Pramod and C. Renuka, *J. Fluoresc.*, 2025, 1–14.
110 Y. Sun, Y. An, J. Huang and Z. Yin, *Dyes Pigm.*, 2025, **236**, 112661.